Valorisation of carbon-rich solid wastes into nanostructured catalysts for wet peroxide oxidation of contaminants of emerging concern

Lucas Fenato Sanches

Thesis report presented to

Escola Superior de Tecnologia e Gestão

Instituto Politécnico de Bragança

to obtain a master's degree in

Chemical Engineering

within the scope of the double diploma with

Universidade Tecnológica Federal do Paraná

Supervisors

Prof. Dr. Helder Teixeira Gomes

Prof. Dr. Fernando Alves da Silva

Dr. Jose Luis Diaz de Tuesta Triviño

Bragança

2021

ACKNOWLEDGEMENTS

I thank God to give me the capacity, health, persistence and opportunity to accomplish this role work, never letting me alone and keeping me up every day even away from family and friends.

During all the time my family supported me, gave me motivation and conditions in every moment, so I also kindly would like to thank them.

My friends also deserve my acknowledgements for the company and support during the difficult days, making me feel at home all this time.

I thank the researchers that were always with me during the lab days, Adriano dos Santos Silva and Fernanda Fontana Roman, for the availability and energy to support and teach me everything I needed.

I would like to especially thank my supervisors Fernando Alves da Silva, Jose Luis Diaz de Tuesta Triviño and Helder Teixeira Gomes for all the support and time given during all this work, helping with the quality of this work, clearing all doubts I had and for the opportunity given to work with the exemplary professionals they are.

Finally, I thank UTFPR and IPB for all the structure, receptibility and opportunities that made me grow and develop a lot with this work.

This work is a result of project PLASTIC_TO_FUEL & MAT, with reference POCI-01-0145-FEDER-031439 and CIMO - UIDB/00690/2020 financed through FCT/MCTES (PIDDAC).

Abstract

This work deals with the application of carbon nanotubes (CNTs) and graphene oxide (GO) in the catalytic wet peroxide oxidation (CWPO) of paracetamol (PCM), a pharmaceutical compound selected as model contaminant of emerging concern (CEC). CNTs were synthetized by catalytic chemical vapor deposition (CVD) at 850 ºC, considering low-density polyethylene (LDPE), high-density polyethylene (HDPE), and polypropylene (PP) as carbon precursors representative of urban plastic solid waste. The yield of the CNTs production was about 24% for PP, 22% for LDPE and 18% for HDPE. Part of the amount produced of CNTs were washed to evaluate changes in the catalytic activity, generating the carbon nanotubes washed (CNTWs). The washing process caused weight losses of 64% in CNT_HDPE, 51% in CNT_PP and 41% in CNT_LDPE. Iron oxides supported in alumina (IO@Al_2O_3) nanoparticles previously synthesized by sol-gel were used as catalysts in the CVD process. GO was received from a partnership of the group. There were made characterizations of FTIR, S_{BET} and ash content. By the FTIR and ash content, it was found that CVD process could keep Fe inside the structure of the CNTs and the washing process kept a parcel of Fe inside them. The S_{BET} revealed a difference among the area between the nanotubes, indicating different structural properties of them, where CNT_PP showed the biggest area of the CNTs, GO presented the lowest area and IO@Al_2O_3 the highest area of the materials. The catalysts, including CNTs, CNTWs, GO and IO@Al_2O_3, were tested in the CWPO of PCM at 80 ºC, C^0_{PCM} = 100 ppm, $C^0_{H_2O_2}$ = 472 mg L^{-1}, pH_0 = 3.5, and $C_{catalyst}$ = 2.5 g L^{-1}, monitoring during 24 h the concentration of PCM, H_2O_2, aromatic and phenolic compounds, and intermediates identification. All the materials showed activity allowing to decompose completely the pharmaceutical in aqueous solutions until 1440 min. In particular, the CNTs synthesized from HDPE lead to complete removal of the pollutant after 30 min of reaction and the CNTWs synthesized from LDPE lead to complete removal until 360 min. GO presented a good PCM degradation capacity, however presented a considerable formation of refractory intermediates. IO@Al_2O_3 also presented good catalytic activity, but the high content of Fe can potentially cause a leaching problem. Finally, the catalyst with the highest activity and lower inorganic catalysts content was CNTW_LDPE, which was tested about its reusability. Thus, 3 runs were made and the catalyst proved to keep its activity, being capable to degrade all of the pollutant after 24 h.

Keywords: Contaminants of emerging concern, carbon nanotubes, graphene oxide, advanced oxidation processes, plastic waste.

Resumo

O trabalho trata do desenvolvimento da aplicação de nanotubos de carbono (CNTs) e óxido de grafeno (GO) na oxidação catalítica úmida com peróxido (CWPO) do paracetamol (PCM), um fármaco selecionado como modelo de um contaminante de preocupação emergente (CEC). Os CNTs foram sintetizados por deposição química a vapor (CVD) a 850 °C, utilizando-se como fonte de carbono os polímeros polietileno de baixa densidade (LDPE), polietileno de alta densidade (HDPE) e polipropileno (PP), sendo estes representantes de resíduos plásticos carbonosos. O rendimento da produção de CNTs foi de 24% para o PP, 22% para o LDPE e 18% para o HDPE. Parte dos CNTs produzidos passaram por um processo de lavagem, para que pudesse ser comparada as atividades catalíticas antes e após a lavagem, gerando os nanotubos de carbono lavados (CNTWs). O processo de lavagem causou perdas de massa de 64% no CNT_HDPE, 51% no CNT_PP e 41% no CNT_LDPE. Nanopartículas de óxidos de ferro suportadas em alumina (IO@Al_2O_3) foram previamente sintetizadas por método de sol-gel e utilizadas como catalisador no processo de CVD. O GO utilizado no trabalho foi adquirido por um projeto de colaboração com outro grupo de pesquisa. Foram feitas caracterizações dos materiais por FT-IR, teor de cinzas e S_{BET}. Pelo FT-IR e teor de cinzas, pode-se visualizar que o processo de CVD pode manter o Fe dentro da estrutura dos CNTs e o processo de lavagem manteve uma parcela de Fe dentro dos materiais. As análises de SBET mostraram uma diferença entre as áreas dos diferentes CNTs, indicando propriedades estruturais diferentes entre eles, onde o CNT_PP mostrou a maior área entre os CNTs, o GO a menor área e o IO@Al_2O_3 a maior área dentre todos os materiais. Os materiais, incluindo os CNTs, CNTWs, GO e IO@Al_2O_3 foram testados nos processos de CWPO do PCM a 80 °C, C^0_{PCM} = 100 ppm, $C^0_{H_2O_2}$ = 472 mg L^{-1}, pH_0 = 3.5 e $C^0_{catalisador}$ = 2.5 g L^{-1}, sendo monitorizados, durante 24 horas, os parâmetros de concentração de PCM, H_2O_2, formação de compostos aromáticos e fenólicos, e identificação de intermediários. Todos os materiais mostraram atividade catalítica, permitindo a decomposição completa do fármaco em soluções aquosas em até 24 h. Em particular, o CNT_HDPE mostrou o melhor rendimento entre os CNTs, levando a remoção completa do poluente depois de 30 min de reação, e o CNTW_LDPE, o melhor dentre os CNTWs, levou a remoção completa após 6 h. O GO mostrou boa taxa de degradação do PCM, porém mostrou grandes formações de compostos intermediários refratários ao processo. O IO@Al_2O_3 também mostrou alta atividade catalítica, porém devido o alto teor de Fe em sua composição, o material tem grande chance de causar lixiviação na solução. Por fim, o catalisador com a maior atividade

catalítica e o menor teor de compostos inorgânicos (catalisador metálico) foi o CNTW_LDPE, o qual foi testado quanto a sua reutilização. Portanto, 3 reações de CWPO foram conduzidas como mesmo catalisador, e o mesmo provou que pode manter sua atividade mesmo após seguidas utilizações, sendo capaz de remover todo o poluente em até 24 h.

Palavras-chave: Contaminantes de preocupação emergente, nanotubos de carbono, óxido de grafeno, processos de oxidação avançada, resíduos plásticos.

TABLE OF CONTENTS

INDEX OF FIGURES

INDEX OF TABLES

LIST OF ABBREVIATIONS

AMR – antimicrobial resistance;

AOPs – advanced oxidation processes;

C – parameter related to the energy of monolayer adsorption;

C_{cat} – catalyst concentration;

CECs – contaminants of emerging concern;

$C_{H_2O_2}$ – hydrogen peroxide concentration;

CNT – carbon nanotube;

CVD – chemical vapour deposition;

CWPO – catalytic wet peroxide oxidation;

D – nanotube diameter;

FCR – Folin-Ciocalteu's reagent;

FTIR – Fourier transform infrared spectroscopy;

GA – gallic acid;

GO – graphene oxide;

HDPE – high-density polyethylene;

HPLC – high-performance liquid chromatography;

IO@Al_2O_3– iron oxides supported on alumina;

Lcat – length of catalyst bed;

LDPE – low-density polyethylene;

M_{cat} – catalyst mass;

Mn – number average molecular weight of the polymer;

MSW – municipal solid waste;

Mw – weight average molecular weight of the polymer;

MWCNT – multi-walled carbon nanotube;

n – specific amount adsorbed;

n_m – specific monolayer capacity;

NCMs – nanostructured carbon materials;

PET – polyethylene-terephthalate;

p/p^0 – relative pressure;

pH_0 – initial pH;

PP – polypropylene;

PVC – polyvinyl chloride;

S_{BET} – BET specific surface area;

S_{ext} – external surface area;

$S_{Langmuir}$ – Langmuir specific surface area;

S_{mic} – microporous surface area;

SWCNT – single-walled carbon nanotube;

TOC – total organic carbon;

$h\nu$ – UV irradiation;

V_{mic} – micropore volume;

W_{mic} – average pore width;

WWTP – wastewater treatment plant;

X_n – degradation level of a given pollutant;

X_{COD} – chemical oxygen demand conversion;

X_{TOC} – conversion of total organic carbon.

INTRODUCTION

1 INTRODUCTION

Contaminants of emerging concern (CECs) are defined as substances that are not listed in the regulatory standards of hazardous components, but these substances can be harmful to aquatic and human life at even trace concentrations [1,2]. CEC can be represented by chemicals, such as household cleaning and personal care products, lawn care, medicines and agricultural products [3]. The problems of CECs arise by the fact that they can't be removed efficiently in conventional treatments used in wastewater treatment plants (WWTPs), thus accumulating in water bodies [4].

Last years, the presence of pharmaceutical compounds in water has been a current theme of studies due to the resistance of microorganisms to the effect of pharmaceuticals and dangerous impact to the environment [5–10]. Usually, pharmaceuticals and CECs are difficult to be degraded by conventional WWTPs, leading to their discharge [11].

Since the common treatment plants are not able to efficiently remove these pollutants, one of the alternative methods of water treatment are the Advanced Oxidation Processes (AOPs). In these treatments, highly oxidizing radicals (HO•) are produced to degrade by oxidation a wide range of water organic pollutants [12].

Municipal solid wastes are another kind of pollutants that is gaining attention by their problems. The problems caused by this kind of pollution affects mainly the urban areas, where the generation of residues is much higher due to industrialization, populational growth and society's lifestyle [13]. Problems attributed to solid wastes include the degradation of environmental quality by the generation of greenhouse gases, leachates and odours [14].

Since solid wastes, such as plastics, lasts many years to be degraded, methods of reuse and valorisation of these residues are acting as impactful alternatives to avoid some of the drastic effects of its wrong disposal.

This work considers the valorisation of polymers by its use as precursors for the synthesis of catalysts and their further use in Catalytic Wet Peroxide Oxidation (CWPO) of waters contamined with pharmaceuticals of emerging concern. The parameters involved in the synthesis of the catalysts and in CWPO are also studied in order to obtain the best yield.

STATE OF THE ART

2 STATE OF THE ART

2.1 Water pollution

The world is facing various water quality deterioration problems due to some leading causes, such as pollution, agriculture, growth of the population, demographic changes, urbanization and economic development [15,16]. By 2025 it is estimated that half of the world's population will be living inside stressed-water areas, thus hundreds of millions of people can be dangerously contaminated [17].

Since there is a growing concern about the problems caused by the polluted water, the management of water quality must be increased to guarantee human health, preservation of the environment and to propitiate a sustainable development [18].

There are many kinds of pollutants found in water, but in the past years, one class of pollutants focused the attention of researchers: the pharmaceuticals. Usually, a significant part of these substances, between 30 to 90% of the oral dose that is taken, is excreted by the endocrine system and destined to wastewater [19]. Every year 100,000 tons of 600 kinds of different active pharmaceuticals are produced, from which Europe corresponds to 24% of the consumption of these products [19].

In addition, WWTPs usually are not able to deal with these kinds of substances, removing only until 70% of them [20]. So, after the treatment, the rest of these chemical compounds are destined to water bodies [21].

The presence of pharmaceuticals in the environment can cause several problems, such as antimicrobial resistance (AMR), which is one of the most hazardous issues to human health [22]. The AMR has caused many deaths in Europe, and the estimative for 2050 is about 390,000 deaths by this cause [19]. Furthermore, pharmaceuticals can cause other several problems in the environment, exemplified by immunotoxicity and bioaccumulation [23].

Pharmaceuticals represent groups of compounds such as anti-inflammatories, antibiotics, blood lipids, antiepileptics, hormones, tranquilizers, X-ray contrast, regulators, contrast media and cytostatic drugs [21,24].

Inside the classes of pharmaceuticals, some deserve more attention for its higher risks to the environment, namely diclofenac, ibuprofen, sulfamethoxazole, paracetamol, ethinylestradiol, paraxanthine, atorvastatin, carbamazepine, estriol, venlafaxine, ranitidine, spiramycin, zidovudine and amoxicillin [25,26]. Considering the components above,

diclofenac and ethinylestradiol were recently added into the watch list of the European Union monitoring [27]

A pharmaceutical that is also found in natural waters is the paracetamol, which are also extensively used as a painkiller since is analgesic [28]. This substance is composed by the functional groups of hydroxyl, benzene and amide group, as can be seen in the molecule pictured in Figure 1 [29].

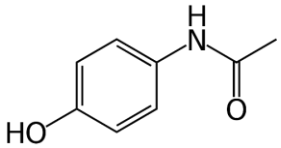

Figure 1 - Paracetamol structure

A review showed that 284 substances were found in concentrations above the detection limits in rivers from Europe, from which 73 were antibiotics and fungicides, 30 anti-inflammatories and analgesics, 20 anticonvulsants and anxiolytics, 19 antihypertensives, 19 antidepressants, 13 steroids and hormones, 7 antiviral drugs, 5 diuretics, and others 66 pharmaceuticals, proving the need of actions to be done to avoid this imminent risk [25].

2.2 European, Portuguese and Brazilian law

Table 1 - Brazilian and Portuguese standards of water disposal

Parameter	Value	
	Brazil	Portugal
pH	5 - 9	6 - 9
Temperature	< 40 ºC	Maximum increase of 3°C in the receptor water body temperature
BOD 5	< 120 mg/L	< 40 mg/L
Fe	15.0 mg/L	2.0 mg/L
Phenols	0.5 mg/L	0.5 mg/L

Source: Adapted from [30] and [31].

The Brazilian regulation about the contaminants in wastewater follows the CONAMA (National Environment Council) resolution nº 430/2011, that stipulate standard conditions of disposal waters, and some of them is presented in Table 1 [30]. In Europe, each country establishes its standards of composition for wastewater, following the European Directive n.º 91/271/CEE [32]. In Portugal, the limits follow the decree-law n.° 236/98 and are also presented in Table 1 [31].

2.3 Water and wastewater treatments

Effluent water treatment can be classified into four stages: pre-treatment, primary, secondary and tertiary. The pre-treatment is usually considered with the primary treatment, including treatments as large particle removal, neutralization, grease separation, grit removal, flotation, flocculation, coagulation and sedimentation. Secondary treatments include biological treatments as aerobic and anaerobic and activated sludge process followed by sludge treatment. Tertiary treatment is not generally used but includes treatments as nitrification, membrane processes, adsorption processes and advanced oxidation processes (AOPs). The tertiary treatment represents an important mean for the removal of heavy metals, refractory organics, pathogens, and chemicals, those that are not efficiently removed in the previous treatments. [33–35]. The common treatments of the WWTPs, such as flocculation, filtration and biological treatment, can't remove them efficiently [36–39].

A review related the efficiency of pharmaceuticals removal reported in the literature in WWTPs, showing the high persistency of pharmaceuticals, exhibiting maximum degradation values of 75% for diclofenac, 95% for ibuprofen and 45% for carbamazepine. [24].

Another review about the presence of pharmaceuticals in WWTPs effluents in Europe exhibited high occurrences and average concentrations of carbamazepine, ibuprofen, sulfamethoxazole and diclofenac. For these pharmaceuticals, the values were, respectively, 832 ng L^{-1} and 90%, 80.5 ng L^{-1} and 57%, 280 ng L^{-1} and 83%, 49.5 ng L^{-1} and 89% [40]. Paracetamol has also been reported in the literature in considerable concentrations (< 9.5 µg L^{-1}) in WWTPs effluents and surface waters in many different places of the world [41–45].

Many WWTPs effluents show higher values than the average mentioned, leading to the dangerous persistency of these compounds in water, which means that they are hazardous principally in concentrations above µg L^{-1} [46,47].

2.4 Advanced oxidation processes

AOPs have demonstrated high capacity in the treatment of pollutants even in trace levels, having the possibility to be applied in many fields, especially in municipal wastewater and groundwater treatments [48]. Previous studies showed interesting results of micropollutants degradation, such as pharmaceuticals, pesticides, dyes, and solvents, being capable to oxidize all the remaining pollutants for tertiary treatments [49–53]. AOPs have demonstrated high importance for scientific knowledge since the remaining pollutants of the WWTPs need to be treated to avoid hazardous effects in the water dependences.

AOPs are used to achieve the highest oxidation of the organic compounds, using the generation of $HO^{\bullet}$ radicals, operating at pressures and temperatures near the ambient [54–56]. The highly oxidizing radicals will be responsible for the degradation of the pollutants into CO_2, water and other products from the pollutant degradation [57,58].

The main processes used in AOPs are ozonation, photolysis, photocatalysis, Fenton, and electrooxidation [46,59–61].

The ozonation process can be done by direct and indirect methods. The direct method works by the oxidation of the pollutant by the natural O_3 oxidant capacity [62]. Otherwise, the indirect method uses the decomposition of ozone to produce $HO^{\bullet}$ radicals, initiating chain reactions to generate the radicals and to promote the process (Equations 1 and 3) [46]. The indirect method generally uses the addition of H_2O_2 to generate HO_2^- ions and consequently $HO^{\bullet}$ radicals (Equations 2 and 3), which increases ozone decomposition [53,63,64]. This process can be very efficient to degrade pharmaceuticals, then it turns capable to totally degrade compounds, such as sulfamethoxazole [51].

$$O_3 + OH^- \rightarrow HO_2^- + O_2 \quad (1)$$

$$H_2O_2 \rightarrow HO_2^- + H^+ \quad (2)$$

$$HO_2^- + O_3 \rightarrow HO^{\bullet} + O_2^- + O_2 \quad (3)$$

AOPs based on UV, that includes photolysis and catalytic photolysis, act by the reaction between UV irradiation and oxidants, such as H_2O_2, since the molecules of the oxidant agent are cleaved and generates $HO^{\bullet}$ radicals (Equation 4) [53]. The use of lamps in

place of solar UV light is also used in order to perform higher degradation of the oxidants, such as H_2O_2, which presents absorbance in wavelengths near 254 nm [48]. To achieve better efficiencies, metallic-based catalysts are also used to generate excited electrons and positive sites that will further generate $HO^{\bullet}$ and $^{\bullet}O_2^-$ radicals, to enhance the oxidation of organic compounds [51].

$$H_2O_2 + h\nu \rightarrow 2\ HO^{\bullet} \quad (4)$$

Electrooxidation is a process where the oxidizing radicals are formed due to the action of an electric current. The formation of the radicals can be done directly or indirectly. In the direct method, the anode of the electric system will be responsible to remove electrons from the organic pollutant to form small non-toxic compounds. Otherwise, in the indirect method, anions present in the reaction react with the anode of the electric system, generating intermediary oxidizing radicals, such as $HO^{\bullet}$, that will further oxidize organic pollutants [51].

One of the most well-succeeded and more studied AOP in the last years is the use of H_2O_2 and iron salts, the so-called Fenton process [56]. The Fenton process consists in the use of iron compounds, due to its economic concerns, in addition to H_2O_2 as a source of hydroxyl radicals by its degradation [65,66].

The Fenton reaction presents a high reaction rate, demonstrating values of reaction time until 95% lower than other AOPs [62]. The process consists in the oxidation of Fe^{2+} to Fe^{3+} due to the presence of H_2O_2 in an acid solution, *i.e.* pH 2.5-3.0 (Equation 5) [12,56,65]. The oxidation of Fe^{2+} promotes the formation of $HO^{\bullet}$ radicals, which are unselective oxidants. As a result, many reactions may be performed from the beginning of the formation of the radicals [54]. Subsequently, the Fe^{3+} ions formed react with other H_2O_2 molecules to generate $HO_2^{\bullet}$ radicals (Equation 6). The $HO_2^{\bullet}$ radicals formed can react with Fe^{3+} ions to form O_2 and H^+ (Equation 7) [67].

$$Fe^{2+} + H_2O_2 \rightarrow Fe^{3+} + HO^- + HO^{\bullet} \quad (5)$$

$$Fe^{3+} + H_2O_2 \leftrightarrow Fe^{2+} + HOO^{\bullet} + H^+ \quad (6)$$

$$Fe^{3+} + HOO^{\bullet} \rightarrow Fe^{2+} + O_2 + H^+ \quad (7)$$

However, the Fenton process usually generates a considerable amount of sludge, also it is very sensible to pH changes, and it can form complexes with other substances during the reaction, which changes directly the yield of the process and demands additional processes [68,69]. Thus, a change to this method, *i.e*. the use of heterogeneous catalysis, is an possible and interesting alternative to the method, since it allows catalyst recovery, avoid sludge treatments, and higher range of operation if compared with homogeneous [70].

The heterogeneous Fenton, also known as CWPO process, consists in the use of solids to support Fe catalysts that bring the advantages of recovering, regeneration and reuse of the catalyst [71].

However, the concentration of the H_2O_2 used in AOP processes need to be very accurate, since scavenger reactions can occur in high levels if excess of H_2O_2 are considered [48]. Scavenger reactions decrease the effectiveness of oxidative processes since they remove $HO^{\bullet}$ radicals of the reaction (Eqs. 8 to 10).

$$HO\bullet + H_2O_2 \rightarrow HOO^{\bullet} + H_2O \quad (8)$$

$$HOO^{\bullet} + H_2O_2 \rightarrow HO^{\bullet} + H_2O + O_2 \quad (9)$$

$$HOO^{\bullet} + HO_2^{\bullet} \rightarrow H_2O_2 + O_2 \quad (10)$$

2.5 CWPO

Catalytic wet peroxide oxidation consists in a process where a catalyst is used to propitiate the decomposition of H_2O_2 and the formation of the reactive $HO^{\bullet}$ and $HOO^{\bullet}$ radicals [12].

Even though iron is one of the cheapest transition metals, others can be used as catalysts in CWPO for the formation of $OH^{\bullet}$ radicals from H_2O_2, such as Cu, Co, Fe, Al, Zn and Ni [72–76].

The employ of supports to the transition metals in CWPO is one of the main characteristics of this process, so many types of porous supports have been developed including pillared clays, alumina, activated carbons and zeolites [77–81].

The reactional parameters of CWPO can vary between the needs of each process, as can be seen in Table 2. The typical operating conditions are initial pH (pH_0) 2 to 7; 25 to

160°C; 1 to 10 bar; 0.2 to 5 g L^{-1} catalyst concentration; and a dose of H_2O_2 from 50 to 200% of the quantity needed to mineralize the organic matter contained in wastewater [60,82,83].

The main costs are attributed to H_2O_2 [84]. Studies made for cost analysis have shown values of H_2O_2 varying from 0.23-0.41 € kg^{-1}, and the entire processes about 1.6 € m^{-3} of treated wastewater in CWPO processes, depending the amount of organic compounds needed to be degraded [82,84,85].

In continuous processes, the catalyst's costs can be negligible, same in batch cases with the use of heterogeneous catalysts. The possibility of catalyst recovery act as an important role because the price of the catalyst is also included in the entire price of the homogeneous processes, since the large amount of sludge formed in the process need to be treated [84–86]. Thus, strategies to develop more stable catalysts are very relevant to ensure low values of metal leaching and the possibility of reuse.

Table 2 - Scope of nanostructured carbon materials in CWPO.

Catalyst	Model pollutant	Operating CWPO conditions	Best measured result	Reference
Iron-loaded carbon nanotube-microfibrous composite (Fe_2O_3-CNT-MF) (D: 10-30 nm)	1 g L^{-1} of m-cresol	Temperature = 30-90 °C L_{cat} = 1-4 cm bed height $C_{H_2O_2}$ = 3-12 g L^{-1} Time on stream = 6 h	$X_{m\text{-}cresol}$ = 100% X_{TOC} = 50.7% Leached Fe = 1.5 mg L^{-1}	[87]
CuS nanocrystals added with reduced graphene oxide (CuS NCs/rGO)	10 mg L^{-1} of methylene blue	pH_0 = 3.0-11.0 Temperature = 25 °C C_{cat} = 200 mg L^{-1} $C_{H_2O_2}$ = 5.0 mol L^{-1}	$X_{methylene\ blue}$ = 93.1%	[88]
Iron-loaded microfibrous entrapped carbon-nanotube (Fe_2O_3-MF-CNT) (D: 50-100 nm)	1 g L^{-1} of m-cresol	pH_0 = 5.0 Temperature = 40-80 °C $C_{H_2O_2}$ = 6 g L^{-1}	$X_{m\text{-}cresol}$ = 99% X_{TOC} = 47% Leached Fe ≈ 0 mg L^{-1}	[89]
Au nanoparticles supported on a hydrophobic CNT (Au/CNT) (D: 5.8 nm)	50 mg L^{-1} of methylene blue	pH_0 ~ 7.0 C_{cat} = 500 mg L^{-1} $C_{H_2O_2}$ = 125-500 mmol L^{-1}	$X_{methylene\ blue}$ = 100% Leached Au = 30%	[90]
Fe_3O_4 nanoparticles-decorated reduced graphene oxide magnetic nanocomposite (Fe_3O_4/rGO NCs)	10 mg L^{-1} of methylene blue	pH_0 = 3-11 Temperature = 25 °C M_{cat} = 30 mg $C_{H_2O_2}$ = 60 mmol L^{-1} time = 120 min	$X_{methylene\ blue}$ ≈ 100% X_{TOC} = 28.5% Leached Fe < 1.16 mg L^{-1}	[91]
Magnetic magnetite/multi-walled carbon nanotube (Fe_3O_4/MWCNT) (D x L: 30-50 nm x 20 μm)	10.0 mg L^{-1} of diclofenac	pH_0 = 6.7 Temperature = 40-60 °C C_{cat} = 0.5-1.0 g L^{-1} $C_{H_2O_2}$ = 1.0-2.7 mmol L^{-1} time = 3 h	$X_{diclofenac}$ = 95%	[92]

Table 2 – (continued)

Catalyst	Model pollutant	Operating CWPO conditions	Best measured result	Reference
Fe_3O_4/MWCNTs (D: 10-30 nm)	100 mg L^{-1} of methyl orange	Temperature = 20-60 °C C_{cat} = 1-5 g L^{-1} $C_{H_2O_2}$ = 9.69-48.45 mmol L^{-1} pH = 1.0-5.0 time = 60 min	$X_{methyl\ orange} \approx 100\%$	[93]
Fe-catalyst in nine different supports: 1. CNTs 2. carbon nanofibers 3. activated carbon 4. hydritalcite 5. mesoporous silica 6. silica 7. silica xerogel 8. sepiolite 9. zeolite USY	Acid orange II textile dye (AOII)	pH_0 =3.0 Temperature = 30°C $C_{H2O2/AOII}$ = 5 w/w M_{cat} = 0.5 g time = 120 min	X_{AOII} = 100% X_{TOC} = 65% X_{COD} = 75% Leached Fe < 58.3%	[94]
Microfibers entrapped carbon-nanotube composite catalyst with iron loaded (MF-CNT-Fe_2O_3)	1 g L^{-1} of m-cresol	Temperature = 80 °C M_{cat} = 2 cm bed height $C_{H_2O_2}$ = 6 g L^{-1} time = 6 h	$X_{m\text{-}cresol}$ = 99% X_{TOC} = 42% Leached Fe = 0.25 mg L^{-1}	[87]
Monolayer graphene film (Gr)	1.0 g L^{-1} of phenol	Temperature = 30-90 °C M_{cat} = 1-4 cm bed height $C_{H_2O_2}$ = 5.1 g L^{-1} time = 72 h	X_{phenol} = 100% X_{TOC} = 91%	[95]
Activated carbons, carbon multiwalled-nanotubes (O.D × I.D. × L: 10–15 nm × 2–6 nm × 0.1–10 μm), glycerol-based carbon materials and carbon xerogels	100 mg L^{-1} of 2-nitrophenol	pH_0 = 3 Temperature = 50 °C C_{cat} = 0.1 g L^{-1} $C_{H_2O_2}$ = 34.6 mM time = 150 min	$X_{2\text{-}nitrophenol}$ = 90% X_{TOC} = 13% Leached Fe < 2.97 mg L^{-1}	[96]

Table 2 – (continued)

Catalyst	Model pollutant	Operating CWPO conditions	Best measured result	Reference
Reduced graphene oxide (rGO)	5 g L^{-1} of 4-nitrophenol	pH_0 = 3 Temperature = 50°C C_{cat} = 2.5 g L^{-1} $C_{H_2O_2}$ = 17.8 g L^{-1} time = 24 h	$X_{4\text{-}nitrophenol}$ = 65% X_{TOC} = 23%	[97]
Multiwalled CNTs, carbon nanofibres, high surface area graphite, and activated carbons	200 ppm of C.I. Reactive Red 241 dye	pH_0 ~ 3.5 Temperature = 25°C C_{cat} = 2.16 g L^{-1} $C_{H_2O_2}$ = 1 mol L^{-1} time = 3 h	X_{dye} = 100%	[98]
Graphite oxide (GrO) with HKUST-1 composites	100 mg L^{-1} of phenol	pH_0 = 4-9 Temperature = 40-80 °C C_{cat} = 0.2 g L^{-1} $C_{H_2O_2}$ = 0.46 mL (30 wt%)	X_{phenol} = 100% X_{COD} = 93%	[99]
Magnetite/multi-walled carbon nanotubes (Fe_3O_4/MWCNTs) (D: <50 nm)	10.0 mg L^{-1} of naproxen	pH_0 = 5-9 Temperature = 30-70 °C C_{cat} = 1.0 g L^{-1} $C_{H_2O_2}$ = 0.5-2.5 mM time = 3 h	$X_{naproxen}$ = 100% $X_{TOC} \approx$ 50%	[100]
Graphene-based MnO_2 coated carbon nanotubes (D: 5-35 nm)	20-100 mg L^{-1} of basic red 18 dye	pH_0 = 3-8 Temperature = 30-70 °C C_{cat} = 0.25 g L^{-1} time = 150 min	$X_{basix\ red\ 18\ dye}$ = 100%	[101]
Commercial MWCNTs: 1. SA1 (O.D.×I.D.×L: 10–15 nm × 2–6 nm × 0.1–10 µm) 2. SA2 (O.D.×L: 6–9 nm × 5 µm) 3. NC (O.D.×L: 9.5 nm and length of 1.5 µm) 4. SZ (O.D.×L: <10 nm × 5–15 µm) 5. LSZ (O.D.×L: 60–100 nm × 5–15 µm)	4.5 g L^{-1} of phenol	pH_0 = 3.5 Temperature = 80 ºC C_{cat} = 2.5 g L^{-1} $C_{H_2O_2}$ = 25 g L^{-1} time = 24 h	X_{phenol} = 80% X_{TOC} = 77.7% Leached Fe = 25 mg L^{-1}	[12]

2.6 Nanostructured carbon materials in CWPO

Nanostructured carbon materials (NCMs) are used in several areas of study, such as adsorption, catalysis, supercapacitors, degradation of organic matter and substance host [102–104]. Some NCMs are graphene, carbon nanofiber and CNT, those that have its own characteristic properties, morphology and importance for the catalysis field [105].

Graphene, that was firstly reported by Novoselov et al. [106] can be described as a two-dimensional one-atom-thick planar sheet of sp^2-bonded hybridized carbon atoms in a two-dimensional honeycomb lattice [107,108]. Besides graphene has unique properties, such as large specific surface area, abundant surface functional groups and high colloidal stability and the thinnest and strongest material ever been measured [108,109].

The characteristics of the graphene are favourable to catalytic reactions, particularly the absence of metals in its common production that avoids metal leaching and the superior electron mobility that are favourable to the occurrence of reactions [105].

The CNTs was firstly reported and analysed in a study of the structure of nanotubes grown in electrodes [110]. This carbon material showed properties such as high mechanical resistance, low mass-transfer limitations, high level of order, high thermal stability and specific electronic properties [12].

The CNTs can be classified into two types: single-walled carbon nanotubes (SWCNTs) and multi-walled carbon nanotubes (MWCNTs) [111]. The properties between these classifications can be attributed to the difference in structure and composition, mainly about chirality, structure defects, surface functionality, number of walls and ordering of the walls. Otherwise, MWCNTs are hollow concentric cylinders capped at both ends [112].

SWCNTs were first reported by Bethune et al. [113], that was studying the formation of fullerenes and nanoencapsulation of magnetic crystals, but they found the formation of nanotubes of one wall. These structures are a rolling of graphene sheet into a seamless cylinder, showing smaller diameters (0.5 to 2 nm) if compared with the MWCNTs (internal diameters of 1.7 to 8 nm and external diameters of 10 to 40 nm) [112,114].

Both kinds of CNTs can be synthesized by two forms: directly by other carbon structures, such as graphene and fullerene, and by catalytic reactions between carbon-rich materials. In the second case, there is a metal particle attached to one end of the tube, that is responsible for the propitiation of the carbon deposition [115].

Carbon nanofibres are other carbon material, characterized as a biphasic system of hexagonal entangled graphite crystallites and micropores indexed by the faulty packing of the

crystallite bundle, showing sizes of diameter between 100 to 200 nm and considerable surface area [111,116,117].

Due to the thermal and electric properties, acid and basic resistance, variability of possible shapes, easy recovery, high porosity, large surface area and cheaper costs than other conventional supports, carbon nanomaterials are very suitable to be used as support for catalysts and as catalyst themselves [117,118]. In the literature are reported the use of CNTs and graphene oxide (GO) in CWPO processes in micropollutant removal, such as phenolic compounds, dyes, pharmaceuticals, herbicides, among others [12,47,98,100,101,118]. The results of CWPO in some substances mentioned above can be seen in Table 2.

2.6.1 Synthesis methods of nanostructured carbon materials

The synthesis of CNTs may be done by methods such as laser-ablation, arc-discharge evaporation, high-pressure carbon monoxide technique, solar furnace and chemical vapour deposition (CVD) [110,111,119–121]. CVD shows advantages when compared to other processes, such as the opportunity to be implemented in a continuous process, higher quantities of production, relatively low costs, adaptable to the use of gas, liquid or solid sources, more convenient for large-scale production and low reactional times [114,120,122].

CVD is a process where a carbon source, such as hydrocarbons or polymers, is decomposed and the gases generated are conducted by an inert gas, as nitrogen or argon, to pass through a catalyst. The catalyst will propitiate the formation of nanotubes by the dissociation of the gas into carbon and hydrogen. Thereafter, the dissociated carbon diffuses into the catalyst surface and the CNT growth begins, as can be seen in Figure 2 [123,124]. The most used carbon sources are methane, ethylene, benzene, toluene, isobutane, acetylene, xylene, ethanol, 2-propanol and carbon monoxide [122,123].

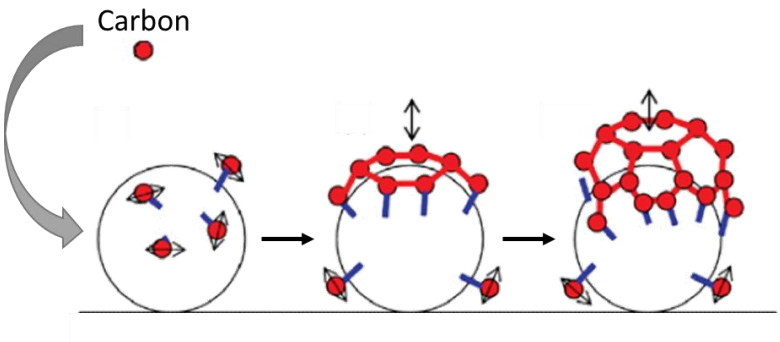

Figure 2 - Representation of the carbon deposition in a catalyst particle. Adapted from [125].

The catalysts used in CVD are usually made of transition metals, such as iron, cobalt, nickel, titanium or the combination of them [120]. The process of carbon deposition in the catalyst can occur by chemisorption, generating a monolayer of carbon, or by physisorption, enabling the formation of multilayer carbon compounds, and the metal particles usually stay at the top or the bottom of the growing nanotubes [114,122]. The interaction between the metal catalyst and its support is also an important parameter since the metal can stay pinned with the support or lifted off, depending on the interaction between both [122].

The conditions of the CVD are very important to the final product since the size of the particles and physical properties change with the temperature, time and gas flows. The values of the reactional parameters can vary between 550 to 1000 °C, 15 to 60 minutes, 50 to 100 mL min^{-1} of inert gases and 10 to 40 mL min^{-1} of carbon source, respectively [122,123,126,127].

2.7 Solid waste management

2.7.1 Valorisation of solid waste into carbonaceous materials

The world produces, every year, 2.01 billion tons of municipal solid waste (MSW), tending to 3.40 billion tonnes in 2050, treating only 66% of these residues [128,129]. The compositions of MSW in the world are mainly organics, followed by paper and plastic, among others. Plastic represents 12% of the total MSWs, *i.e.* 242 tonnes [128,130].

One of the main problems of the treatment of these MSWs is the cost related to efficient waste management, making it harder in developing countries since the costs of MSW treatment can vary between $35-100 per tonne, causing environmental problems by the bad waste disposal [128,131]. In this way, renewable energy sources are an alternative to decrease the problems of MSWs. Many types of research have been made about MSWs reuse to decrease costs, valorisation of residues, produce fuels and generate energy [132].

The treatments used to convert solid wastes to valorised materials can vary depending on the source material. MSWs can be treated by thermochemical, biochemical, and physicochemical processes, generating products, such as alcohols, acids, biodiesel, biogas, metallic precursors, polymers and carbon materials [132–134].

Plastics show unique properties, such as the high content of carbon, allowing their use as a source for carbonaceous materials synthesis. This kind of materials can be represented by polyethylene terephthalate (PET), polystyrene, polypropylene (PP), high-density and low-density polyethylene (LDPE and HDPE), polyvinyl chloride (PVC), among others [135,136].

Thus, the use of plastic wastes as a source of other composites can represent a promising alternative for waste valorisation.

The most used process to degrade plastics is the thermo-chemical process, where pyrolysis is followed by another treatment to transform gases and liquids generated into valorised carbonaceous materials, such as CNTs, GO, carbon nanofibers and carbon charcoal [135].

Thermo-chemical processes usually involve the employment of metal-based catalysts, in order to favour the production of the desired compound [121]. Each catalyst used will drive to different product characteristics related to the structure of the material. A study showed the importance of the particle size of the catalyst in CVD since low particles sizes were favourable to small diameters of CNTs (4 nm) and big cluster particles propitiate higher diameters (20 to 80 nm) [137].

The temperature used in thermo-chemical processes presents fundamental relevance for the desired product material. Diameters, disposition and size of particles can be altered by the difference of temperature of pyrolysis, especially due to the increase of the catalyst particle's mobility when temperature rises [135,138]. In the case of CNTs production, it is notified that lower temperatures (600 to 900 °C) are favourable to carbon MWCNTs production, otherwise higher temperatures (900 to 1200 °C) are favourable to SWCNTs [121].

Another parameter that is very studied is the type of apparatus for the process. The different equipment can be divided by the ones that are only feasible in laboratory scale, such as crucible, quartz tubes and muffle furnace, and the ones that can be constructed for industrial-scale, such as autoclave, moving and fixed bed, and fluidized bed [136]. However, the literature shows that the main parameters that control the quality and yield of the CVD processes are the conditions, such as temperature, time, catalysts, and compositions of the carbon source [136]. Nevertheless, CVD processes that can be scaled-up are gaining more attention, due to their high feasibility in larger productions.

MATERIALS AND METHODS

3 MATERIALS AND METHODS

3.1 Reactants

Ultrapure and distilled water have been used for solutions preparation and washing procedures along this work.

3.1.1 Iron oxides supported in alumina preparation

- Alumina, BASF. Formula: Al_2O_3;
- Ethanol Absolute (99.99%), Fisher Chemical. Formula: C_2H_5OH;
- Ethylene glycol (99%), Fisher Chemical. Formula: $C_2H_6O_2$;
- Iron (II) chloride tetrahydrate, Acros Organics. Formula: $FeCl_2 \cdot 4H_2O$;
- Iron (III) chloride hexahydrate, VWR Chemicals. Formula: $FeCl_3 \cdot 6H_2O$.

3.1.2 Carbon nanotubes synthesis and washing

High-density polyethylene (HDPE), melt index 2.2 g $(10\ min)^{-1}$, Sigma-Aldrich. Formula: $[C_2H_4]_n$;

Low-density polyethylene (LDPE), average Mw ~ 35,000 g mol^{-1}, average Mn ~7,700, Sigma-Aldrich. Formula: $[C_2H_4]_n$;

Polypropylene (PP), average Mw ~250,000 g mol^{-1}, average Mn ~67,000, Sigma-Aldrich. Formula: $[C_3H_6]_n$;

Sulfuric acid (95%), VWR Chemicals. Formula: H_2SO_4;

3.1.3 CWPO of paracetamol and analytical techniques

Folin-Ciocalteu's reagent, PanReac;

Hydrogen peroxide (30%), VWR Chemicals. Formula: H_2O_2;

Orthophosphoric acid (85%), Fisher Chemical. Formula: H_3PO_4;

Paracetamol (98%), Alfa Aesar. Formula: $C_8H_9NO_2$;

Sodium sulphite anhydrous (98%), Panreac. Formula: Na_2SO_3;

Sulfuric acid (95%), VWR Chemicals. Formula: H_2SO_4;

Titanium (IV) oxysulfate (99.99%). Sigma Aldrich. Formula: $TiOSO_4$;

Gallic acid anhydrous. Merck. Formula: $C_7H_6O_5$;

3.2 Synthesis of GO

The GO used in this work was produced by another group in a partnership program. Briefly, the methodology used was an anodic electrochemical exfoliation, where graphites from a Leclanché battery were washed with detergent and distilled water and immersed in a HCl solution (0.1 mol L^{-1}). After, the graphite was polished to the metallic lustre and surface homogeneity. Then, the graphite was used as an electrode, with an area of 4.47 cm^2, and an electrode of silver/silver chloride (Ag/AgCl) was used as a reference. The electrolyte was a solution of sodium fluoride (0.01 mol L^{-1}). For 2 days it was applicated electric currents of 1.5 mA, using an Ivium potenciostat.

3.3 Synthesis of iron oxides-based CVD-catalyst

First, 20 mL of ethanol and 10 mmol of iron (II) chloride tetrahydrate were stirred and heated in a 250 mL two-necked round bottom flask at 80 °C until the boiling point be reached and then cooled to room temperature. In another 250 mL two-necked round bottom flask, 80 mL of glycol ethylene and 20 mmol of iron (III) chloride hexahydrate were stirred and heated at 60 °C for 5 min and then cooled to room temperature. Both previously prepared mixtures and 6.6 g of alumina were put in a 250 mL becker, stirred, and heated at 60 °C for 2 h. The system was heated at 120 °C until the gel texture was achieved. At last, the gel was heated at 210 °C until the dry powder formation, being cooled to room temperature at the end.

The powder synthesized in the previous step was submitted to heat treatment. The sample was calcinated at 300 °C for 12 h and at 600 °C for 24 h in air atmosphere, to obtain the IO@Al_2O_3 catalyst.

3.4 CNT synthesis by CVD

For the CVD process, the furnace showed in Figure 3 was used. The furnace is equipped with 2 crucibles, wherein the first crucible was loaded with 5 g of polymer (LDPE, HDPE and PP), and in the second crucible 1 g of the CVD-catalyst (IO@Al_2O_3) was placed. The working temperature was 850 °C during 1 h with N_2 flow of 50 mL min^{-1}. The synthetized nanotubes were called CNT_LDPE, CNT_HDPE and CNT_PP, according to the polymer used.

Figure 3 - Equipment used for CVD process.

Each CNT produced was washed to remove the remaining IO@Al_2O_3. For this purpose, 1 g of CNT and 50 mL of H_2SO_4 (50%) were stirred and heated at 140 °C during 3 h in a round bottom flask equipped with a condenser. The solid was recovered through filtration and washed with distilled water until the rise water reach the pH of the distilled water. Finally, the CNTs were dried for 12 h at 60 °C in an air oven. The washed nanotubes were called CNTW_LDPE, CNTW_HDPE, and CNTW_PP, respectively, according to the polymer used in their preparation.

To evaluate how efficient was the process, the yield was calculated taking in account the amount of carbon present in the carbon source (polymer) and the carbon present in the structure of the CNTs, determined by an ash content test described below, using the Equation 11.

$$CVD\ Yield = \frac{Carbon\ in\ the\ CNTs\ synthetized}{Carbon\ in\ the\ polymer} x100 \quad (11)$$

3.5 Characterisation of the materials

3.5.1 Surface area analysis

The textural properties of the materials were determined from N_2 adsorption–desorption isotherms at 77 K, obtained in a Quantachrome NOVATOUCH XL[4] adsorption analyzer, following the same procedure as described elsewhere [139]. Briefly, the degasification of the catalysts was conducted at 120 ºC during 16 h and then adsorption isotherms measured. Afterwards, BET (S_{BET}) and Langmuir specific surface area ($S_{Langmuir}$) were determined using BET and Langmuir methods, respectively, as explained above. The total pore volume (V_{Total}) was determined at $p/p_0 = 0.98$. Calculations of those methods were all done by using TouchWinTM software v1.21.

The curves of adsorption were characterized using the updated IUPAC classification of physisorption isotherms [140].

The Equation 12 was used to calculate the S_{BET} and $S_{Langmuir}$.

$$S_i = \frac{n_m . \sigma_m}{V} \tag{12}$$

Where S_i is the specific BET or Langmuir area of the adsorbent, n_m is the volume adsorbed in the monolayer (determined through the BET and Langmuir isotherms), σ_m the molecular cross-sectional area of the N_2 (0.162 nm^2) and V the molar volume of the nitrogen (0.022413995 $m^3\ mol^{-1}$). To determine the n_m parameters, it was used the linear adjustment of the Equation 13 in the case of S_{BET} and Equation 14 in the case of $S_{Langmuir}$.

$$\frac{p/p^0}{n(1-p/p^0)} = \frac{1}{n_m C} + \frac{C-1}{n_m C}(p/p^0) \tag{13}$$

$$\frac{p/p^0}{n} = \frac{1}{C.n_m} + \frac{p/p^0}{n_m} \tag{14}$$

Where p/p^0 is the relative pressure, n is the specific amount adsorbed at the relative p/p^0, n_m is specific monolayer capacity and C is a parameter related to the energy of monolayer adsorption.

The total pore volume was calculated using the Equation 15.

$$Total\ pore\ volume = \frac{n.M_{N_2}}{V_{N_2}.\rho} \quad (15)$$

Where M_{N_2} is the molar mass of N_2, V_{N_2} is the specific volume of N_2, and the value used of ρ was 808000 g m^{-3}.

3.5.2 Fourier Transform Infra-Red spectroscopy (FTIR) analysis

The FTIR spectra of the 9 different samples were recorded on a Perkin Elmer FTIR spectrophotometer UATR Two infrared spectrophotometer, with a resolution of 4 cm^{-1}. The range of wavenumber used in the analysis was from 500 to 4000 cm^{-1}. All the measurements were obtained from the solid samples at room temperature.

3.5.3 Ash content

To evaluate the ash percentage of the materials, a test was conducted adapting the methodology presented elsewhere [141]. Thus, the materials were burnt in a muffle at 550°C until the constant mass was reached in a precision balance (±0.0005). For this evaluation, it was considered the percentage of organic and catalysts fractions, since the materials are composed by a carbonaceous (CNTs) and inorganic structure (CVD-catalysts made of metals used for the growth of the CNTs).

3.6 CWPO of paracetamol

For the CWPO, 100 mL of a paracetamol solution of 100 ppm, at pH adjusted to 3.5 by means of H_2SO_4 solution (0.5 M), was used. The previous solution was added in a 250 mL two-necked round bottom flask equipped with a condenser, and the stoichiometric quantity of H_2O_2 for paracetamol degradation was poured into the system. The mixture remained in agitation at 80 ºC for 5 min, and samples were taken for reference values of the initial concentrations. To start the reaction, 0.25 g of catalyst were added to the system. The apparatus can be seen in Figure 4.

The calculation of the amount of H_2O_2 needed for a stoichiometric reaction with paracetamol was made following the stoichiometric coefficients of Equation 16. The volume of H_2O_2 used in the CWPO of 100 ppm of paracetamol was calculated considering a solution of 30% (w/v) of H_2O_2, which led to a 158 µL of hydrogen peroxide solution.

$$C_8H_9NO_{2\,(aq)} + 21H_2O_{2\,(aq)} \rightarrow 8CO_{2\,(g)} + 25H_2O_{\,(l)} + HNO_{3\,(aq)} \quad (16)$$

During the reaction, samples were collected for the analysis of the TOC, aromaticity, and H_2O_2, phenol and paracetamol concentrations at 0, 15, 30, 60, 120, 240, 360, 480, and 1440 minutes. Each sample of 2.7 mL were withdrawn from the reaction medium for further analysis. After the reaction, the catalyst was washed with distilled water and dried in air oven at 60 °C for 24 h.

Figure 4 - Apparatus used for the CWPO runs.

3.6.1 Adsorption

The adsorption tests were conducted for all the materials in the same conditions of the CWPO, but in the absence of H_2O_2. Instead of previous analysis, the paracetamol concentration was the only conducted for this test since the parameter to be evaluated was the decrease of paracetamol concentration by the adsorption phenomenon. The concentration of the pharmaceutical was conducted in a HPLC with a methodology described in chapter 3.7.1, which deals with the paracetamol concentration evaluation.

3.6.2 Reusability

An interesting parameter to be evaluated is the reusability of the catalyst. This result can show if the catalyst is deactivated after the reactions and if it is possible to reuse them without relevant loss of quality. Thus, it was taken the best catalyst based in the composition and catalytic activity to test its reusability. To this test, the catalyst was washed with distilled water and dried at 60 °C. Then, 2 more CWPO runs was done to evaluate the PCM oxidation and H_2O_2 decomposition and compare with the first run.

3.7 Analytical technics

3.7.1 Paracetamol concentration

For paracetamol concentration measurements, a HPLC Jasco equipped with a UV-VIS detector (UV-2075 Plus) was used, with RES ELUT 5 µm C18-90 Å column (150 mm x 4.6 mm) of VARIAN and a quaternary gradient pump (PU-2089 Plus) for solvent delivery (0.65 ml min^{-1}). For this analysis, a non-isocratic method was used starting with a mixture of H_3PO_4 (0.022 M) and pure acetonitrile (90:10 v/v) fed during 6 min. Then, a gradient elution to reach 65:35 v/v of H_3PO_4 (0.1275% wt) and pure acetonitrile in 5 min was used followed by 20 min at that elution percentage. The wavelength used for the peaked absorbance detection of paracetamol was 277 nm.

3.7.2 H_2O_2 concentration

The method used to determine the concentration of H_2O_2 in the reaction system followed the previous procedure reported in the literature [142]. The method is based in the colorimetric analysis to determine the concentration in the sample. The colour is formed by a yellow compound formation by the reaction presented in the Equation 17 [143].

$$Ti^{4+}_{(aq)} + H_2O_{2\,(aq)} \rightarrow H_2TiO_{4\ (aq)} + H^{+}_{(aq)} \quad (17)$$

For the application of the method a calibration curve was made from the concentrations ranging from 0 to 500 ppm, and the result is shown in Figure 5. For the analysis 1 mL of 0.5 M H_2SO_4 solution, 0.1 mL of $TiOSO_4$ and 1 mL of the sample was added in a volumetric flask of 5 mL and then diluted in distilled water. Subsequently, each

sample was analysed by an UV-VIS spectrophotometry Jasco V-530 at the wavelength of 405 nm.

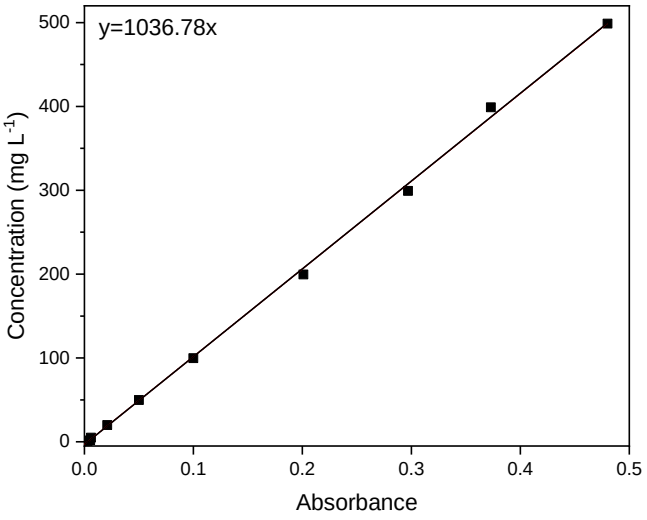

Figure 5 - Calibration curve for H_2O_2 detection.

The linear regression showed an R^2 of 0.9994, which permits a good approximation to the real concentration of the analysis.

3.7.3 Aromatic compounds

The concentration of aromatic compounds formed were quantified using the method described in the literature [144]. Firstly, a buffer solution of H_3PO_4 with pH 7 was prepared to be used as solvent. The analysis consists in the dilution of 0.5 mL of the sample in a volumetric flask of 5 mL and diluted with the buffer solution. Thereafter, the sample was analysed in a UV-VIS spectrophotometry Jasco V-530 at the wavelength of 254 nm.

Since the paracetamol also shows absorbance in the aromaticity test it is necessary to subtract this interference to distinguish the measurement of aromatic compounds and paracetamol. Thus, a calibration curve was made to know the interference of paracetamol in the analysis and is shown in Figure 6.

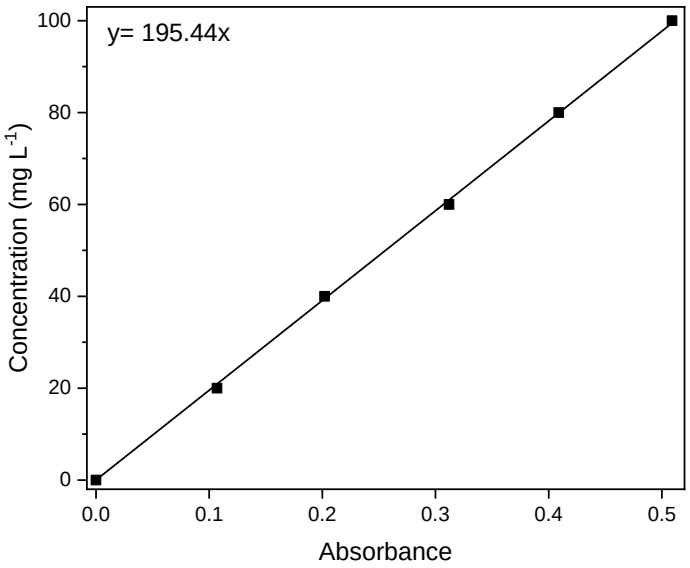

Figure 6 - Calibration curve of paracetamol for aromaticity test

The curve enables the use of the concentration of paracetamol from the HPLC to know the absorbance relative to the concentration of the pollutant, and discount it from the total absorbance of the test, which results in the absorbance of aromatic compounds excluding paracetamol. The amount of aromatic compounds was given in terms of percentage following the Equation 18,

$$\%_t\ of\ aromatics = \frac{ABS_{Total,t} - ABS_{PCM,t}}{ABS_{PCM,0}} \quad (18)$$

Where ABS_{Total} represents the absorbance analyzed and ABS_{PCM} the relative absorbance following the calibration curve mentioned above.

The linear regression showed an R^2 of 0.9998, which gives a good approximation to the paracetamol interference in the analysis of the aromatic compounds in the UV-VIS.

3.7.4 Phenolic compounds

The presence of intermediates as phenolic compounds was quantified adapting the Folin-Ciocalteu's reagent (FCR) methodology presented elsewhere [145]. The test consists in the addition of 0.5 mL of the FCR, 0.5 mL of the sample to be analysed, 2 mL of distilled water, and 0.35 mL of a solution of Na_2CO_3 10% (w/v) in a vial of 10 mL. After the addition of water, the sample was left to stand for 5 minutes. Afterwards, Na_2CO_3 was added, and the

system was left to rest for 1 h. Thereafter, the sample was analysed in a UV-VIS spectrophotometry Jasco V-530 at the wavelength of 765 nm.

To obtain the concentration of phenolic compounds in the sample, a standard curve was made using gallic acid (GA). GA was chosen due to its high interaction with the FCR, being a parameter to correlate the concentration of phenols besides the paracetamol. Besides, this chemical is not present in the reaction of the CWPOs, which represents another good reason to be chosen. Thus, the phenolic compounds were quantified in terms of milligrams of GA per litre, correlating the absorbance values of gallic acid solutions at different concentrations as showed in Figure 7.

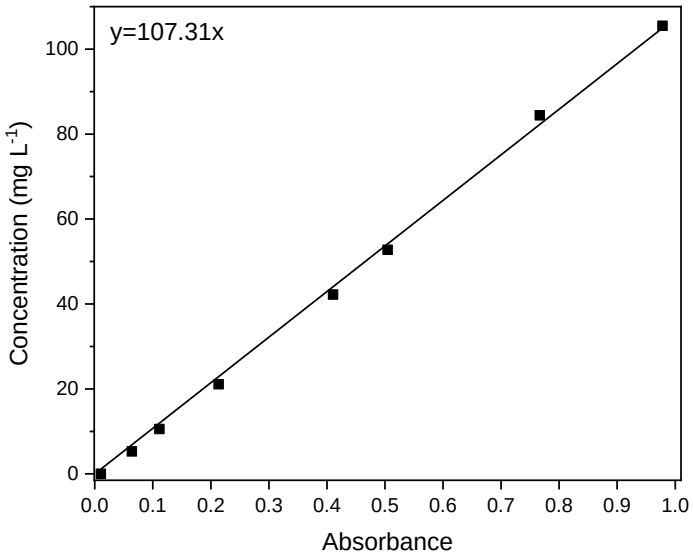

Figure 7 - Standard curve of gallic acid for phenolic evaluation

The linear regression showed an R^2 of 0.9994, giving a good approximation to the relative concentration of gallic acid of the sample.

To verify if paracetamol shows interference in the phenolic analysis a calibration curve was made and is shown in Figure 8. The interference verified was used to discount the absorbance of paracetamol in the sample analysis.

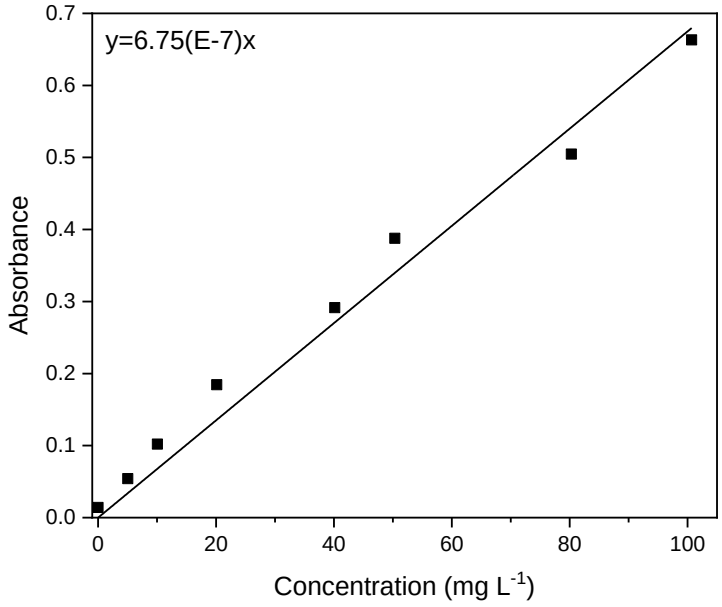

Figure 8 - Calibration curve of paracetamol for phenolic evaluation.

The linear regression showed an R^2 of 0.9901, which allows to a good approximation to the real interference of paracetamol in the analysis.

3.7.5 Detection of intermediates

To better understand the CWPO runs, it was analysed the formation of intermediates during the reaction by means of HPLC detection, the same as the PCM concentration. Previously, some possible intermediates of the process were injected in the HPLC to analyse the residence time of each one, what enables the identification of them during the analysis in the equipment. Thus, each intermediate had its own residence time and could be easily identified.

RESULTS AND DISCUSSION

4 RESULTS AND DISCUSSION

4.1 Characterization of the materials

The synthetized materials were analyzed firstly in terms of production yields and after about their morphological structures, with the use of the methodologies previously covered in chapter 3.5.

4.1.1 Iron oxides supported in alumina synthesis

The prepared material can be seen in Figure 9. The yield of Fe in the sample in relation of the theoretical expected was 21.6%. The material synthetized did not reveal magnetic properties. This fact can be attributed to the formation of maghemite (γ-Fe_2O_3) and/or hematite (α-Fe_2O_3), since both present brown-red colors and are not so magnetic as magnetite, for example. This was expected, since the reaction was made in the presence of atmospheric air, resulting in an oxidative environment [146]. However, after the nanotubes production at high temperatures (850 °C) and inert atmosphere, the particles of CNTs became black and magnetic, as can be seen in Figure 10. This can be explained by a possible reduction of γ-Fe_2O_3 into magnetite under inert atmosphere, fact already related in the literature [147,148].

Figure 9 - IO@Al_2O_3 material prepared by sol-gel.

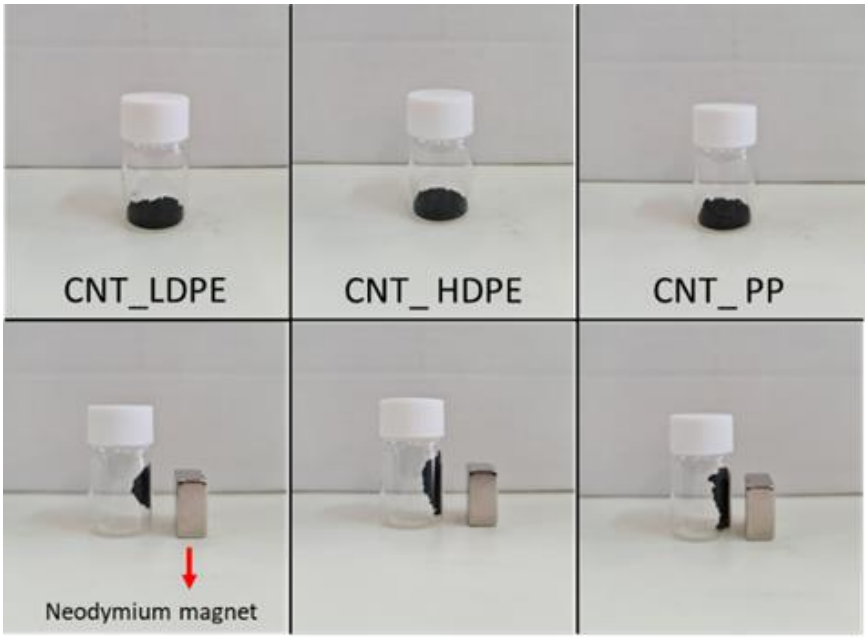

Figure 10 - Magnetism of the produced CNTs.

4.1.2 CNT production yields

The conversion of each polymer into CNTs can be seen in Figure 11. It is possible to conclude that PP has a slightly higher yield, followed by LDPE and HDPE, respectively, agreeing with results reported in the literature with plastics as carbon source [149].

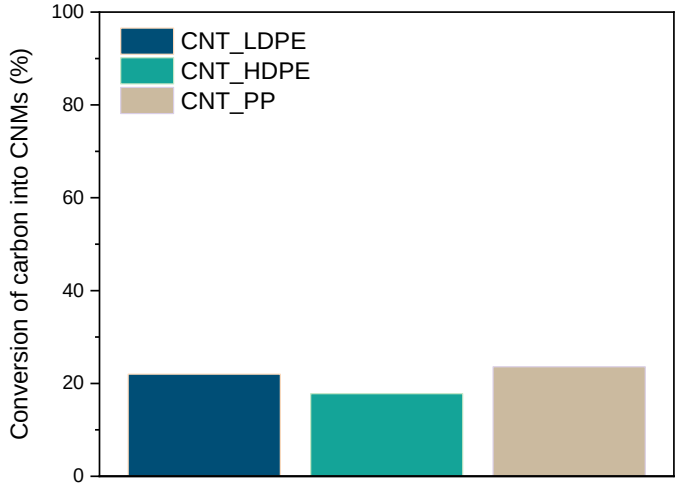

Figure 11 - Carbon conversion of the CVD process before washing.

The values of the conversions were almost the same for the materials considering the standard deviation (1.32% for CNT_LDPE, 2.22% for CNT_HDPE, and 0.82% for CNT_PP). This result showed that although the difference in the composition of generated

gases during the pyrolysis of each polymer, (methane, ethane, ethylene, propane, propylene and butane, among others) the conversions were close [124].

The yield values obtained are close to those found in the literature, where values of 18.8% (LDPE) [150] and 10% (HDPE) [151] have been reported.

The washing process of the synthetized CNTs resulted in a significant weight loss due to the excess of CVD-catalyst particles leaching into the acid solution. The Figure 12 shows the yield of mass loss of each washed CNT.

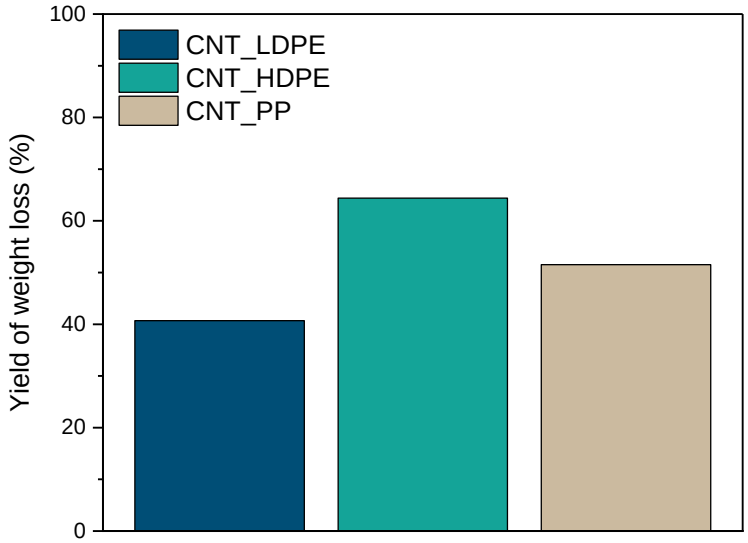

Figure 12 - Weight loss in the washing process.

It is possible to observe that the material CNT_LDPE showed the lowest weight loss, in opposition to that observed in the material CNT_HDPE. These results agree with the yields obtained during the synthesis of the CNTs, since it was expected that the material CNT-HDPE had a rich composition in the CVD-catalyst (by the ash content test presented below), hence higher removals of catalyst per weight should be obtained. This result may indiciate that the material CNT_LDPE has more structure stability than the others, while the material CNT_HDPE is less stable. The structural stability of a catalyst should preferably be high because as long as the material is stable lower quantities of undesirable materials are leached in the solution to be treated.

4.1.3 Ash content

The ash contents of the synthesized materials are presented in Table 3.

With these results it is evident that the washing process remove a lot of the CVD-catalysts present in these materials, since there is a higher ash content in the non-washed

ones. It is also possible to conclude that all the CNTs and CNTWs presented similar compositions, irrespective of the polymer sources.

Table 3 - Composition of the synthesized materials based on the ash content.

Material	Organic content (%)	Ash content (%)	Standard deviation
CNT_LDPE	56.8	43.2	1.4
CNT_HDPE	53.2	46.8	0.2
CNT_PP	65.0	35.0	1.5
CNTW_LDPE	95.8	4.2	0.2
CNTW_HDPE	92.1	7.9	1.2
CNTW_PP	94.3	5.7	0.0
GO	83.1	16.9	0.1

In the case of GO, it was found a relatively high ash content compared with the CNTWs, which means a possible presence of metals from the battery used in the synthesis of this material.

4.1.4 FT-IR analysis

The FT-IR spectra of the IO@Al_2O_3 CVD-catalyst and of the purified and non-purified CNTs are depicted in Figure 13.

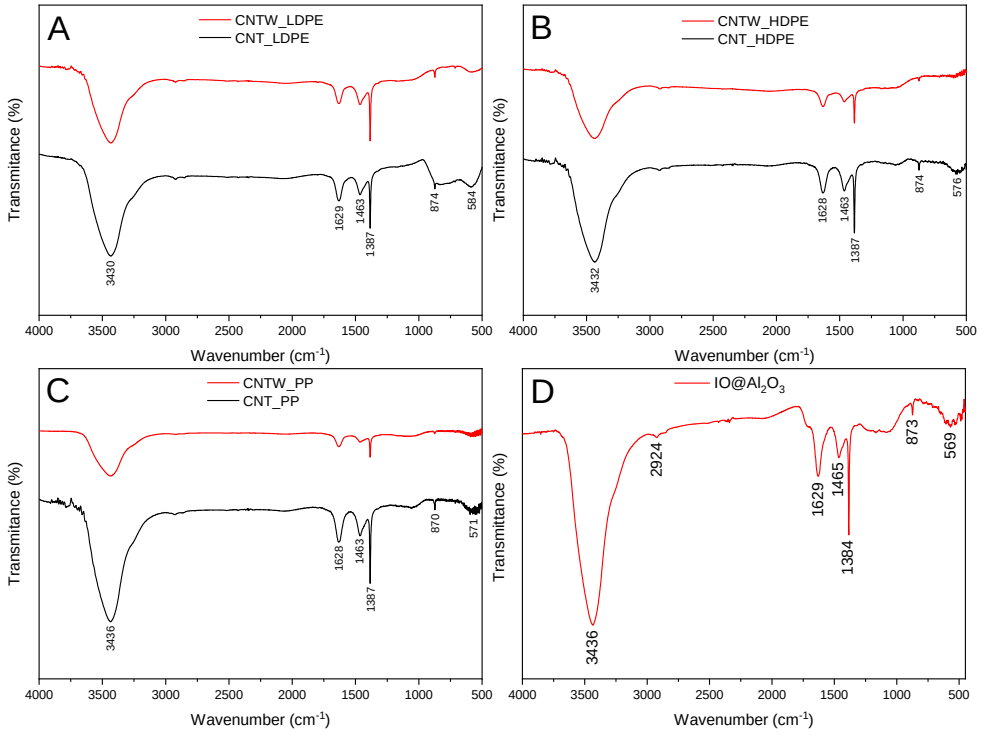

Figure 13 - FT-IR spectra of A) CNTW and CNT of LDPE, B) CNTW and CNT of HDPE, C) CNTW and CNT of PP, and D) IO@Al_2O_3.

It is possible to observe that the FT-IR spectra are very similar among the several materials. Interestingly, the acid-washing process of the carbon nanotubes do not seem to significantly change the materials, since the FT-IR spectra obtained before and after the purification with H_2SO_4 are very similar. No displacement of any bands was observed, which confirms that the washing process did not change the nature of the surface groups of the materials.

In all the spectra it is possible to observe a band between 569 and 584 cm^{-1}, corresponding to the Fe-O stretching vibration, which may be due to the presence of iron oxides [152]. The band between 870 and 874 cm^{-1} can correspond to the C-O functional groups and Al-O stretching vibrations, due to the presence of alumina [93,153]. The bands at 1387 cm^{-1} indicates the presence of carboxylate groups [154]. At 1463 cm^{-1} appear bands assigned to CH_2 or CH_3 bending vibrations [155]. The bands between 1628 and 1629 cm^{-1} can be attributed to the stretching vibration of C=C double bonds [100] and the bands at 2924 cm^{-1} are ascribed to the anti-symmetrical H-O-H stretching vibrations [156]. The bands found between 3430 and 3436 cm^{-1} are due to the presence of -OH groups and some water adsorbed in the materials [92].

It can be observed that after carbon deposition over the CVD-catalyst IO@Al_2O_3, a displacement is observed in the bands in the range of 873-1375 cm^{-1}, indicating an interaction between Fe-O and Al-O groups with the carbon content of the materials. Although these changes in the wavelength absorption were found, the specific vibration interactions remained after CVD, so no modification of magnetite occurred during CVD.

The spectra of GO shows similar bands to those of the CNTs, as can be observed in Figure 14.

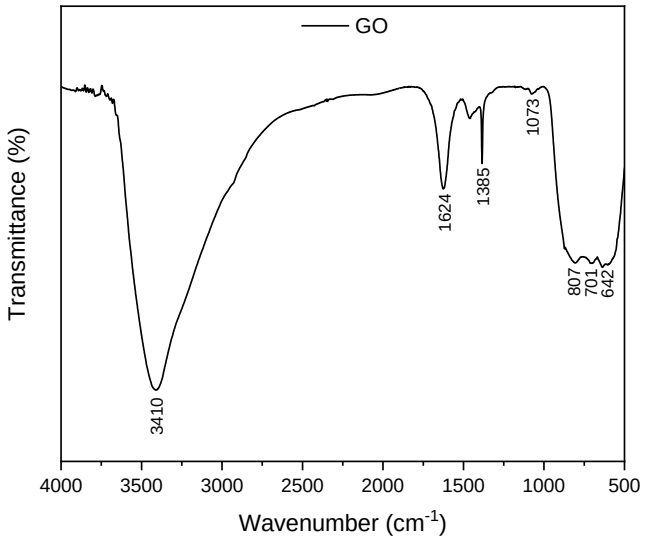

Figure 14 - FT-IR spectra of GO.

In the spectra of GO, the bands between 642 and 807 cm^{-1} are attributed to metallic impurities in the GO precursor [157] and the band at 1073 cm^{-1} suggests the presence of epoxy (-C-O-C-) and alkoxy (C-OH) groups [158]. The band at 1385 and 1624 cm^{-1} represent carboxylic acids (-COOH) and C=C stretching vibrations, respectively [155]. The band at 3410 cm^{-1} represents the O-H stretching vibrations and the water adsorbed in the material [157].

4.1.5 Textural properties

The adsorption and desorption isotherms of N_2 at 77 K obtained with graphene, IO@Al_2O_3 and the carbon nanotubes prior and after their purification are shown in Figure 15.

Following the IUPAC classification, all the materials show a characteristic curve of type II [140]. Since the knee of the curve is almost linear and the adsorption around $p/p_0 = 1$ shows a high increase, the isotherm indicates that the adsorption has a multilayer coverage characteristic. For low relative pressure, a quasi-saturation level on N_2 adsorption was observed, indicating the formation of microporous on the materials.

In the case of the CNTs and CNTWs, shown in Figure 15 A, B, C, D, E and F, the highest adsorption level was achieved with CNTW_PP, indicating a difference in the surface of the material using different carbon sources [150]. The use of polyethylene with different densities appears to promote different morphological characteristics in the surface of the CNTs, since the material CNTW_HDPE shows a higher adsorption capacity than the material CNTW_LDPE. This fact can also be observed in the non-washed materials.

Evaluating the other two materials presented in Figure 15 G and H, it is observed that IO@Al_2O_3 shows similar characteristics to those of the CNTs and CNTWs. Otherwise, GO demonstrated a very low adsorption capacity if compared with the other materials, which is natural due to the characteristics of the carbon layers [158].

The isotherms show a loop of type H3 since they are of type II. This classification indicates that the materials may also be composed by a mesopore network, and the presence of the loop can be associated with capillary and cavitation effects [159,160]. Comparing the materials before washing (Figure 15 A, B and C) and after washing (Figure 15 D, E and F) it is possible to observe that the washing process did not significantly change the pore network of the materials, since they kept similar hysteresis characteristics. This fact can also be evidenced by the S_{BET}, presented in Table 4, where the areas of the materials remain almost the same after the washing process.

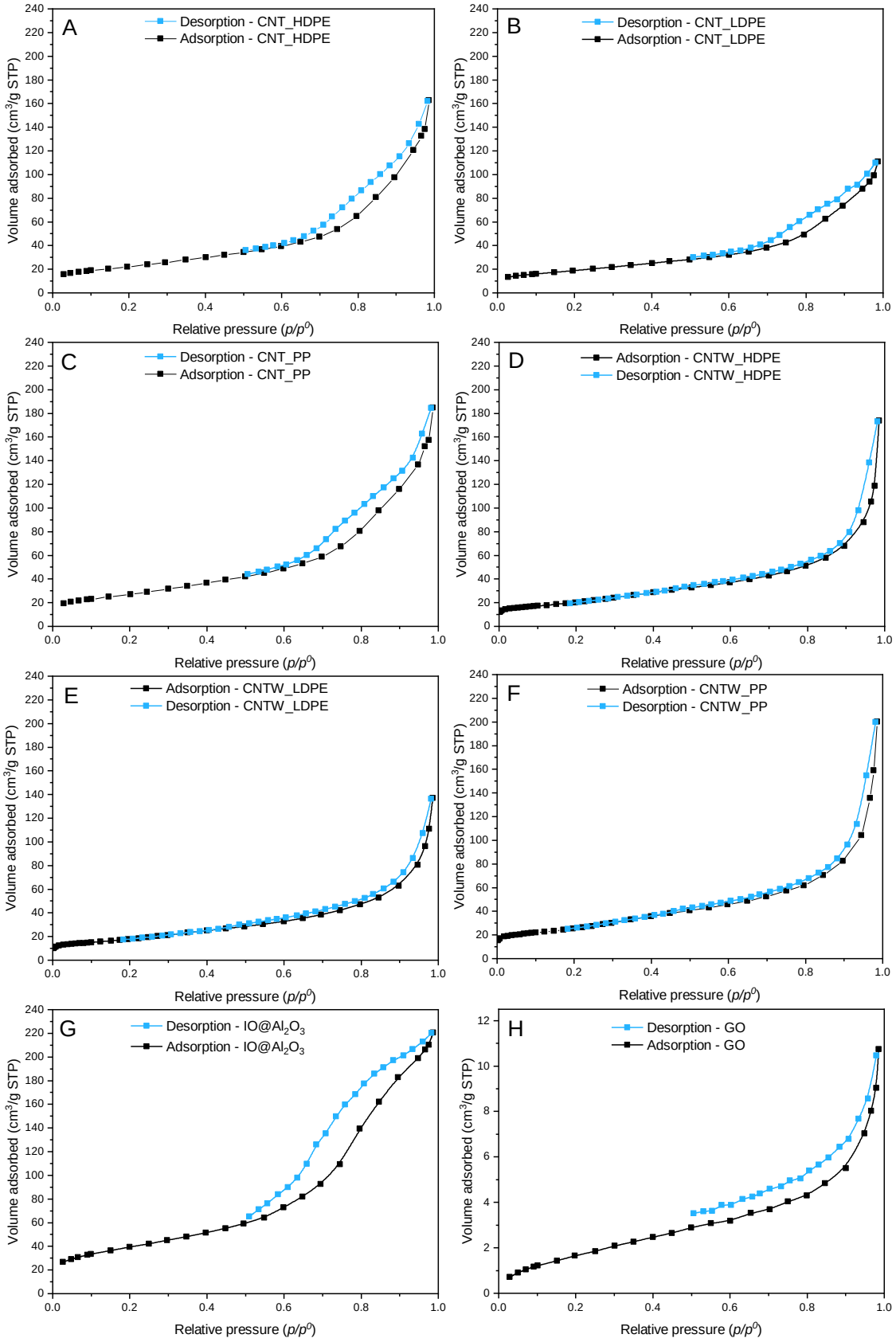

Figure 15 - N_2 adsorption and desorption isotherms at 77 K of A) CNT_HDPE, B) CNT_LDPE, C) CNT_PP, D) CNTW_HDPE, E) CNTW_LDPE, F) CNTW_PP, G) IO@Al_2O_3 CVD-catalyst, and H) GO.

The adsorption and desorption profiles on the materials IO@Al_2O_3 and GO are shown in Figure 15 G and H, respectively. Both materials reveal an H3 loop and similar profiles if compared with the CNTs and CNTWs. In the case of IO@Al_2O_3 the loop was more evident, demonstrating a more retention of the adsorbate and some difference in the structure of the porous if compared with the other materials. Even though GO presents low levels of adsorption, its profile also shows a relatively similar profile to the other materials.

The S_{BET}, $S_{Langmuir}$ and pore volume of the materials can be observed in Table 4.

Table 4 - Textural properties of the produced materials.

Material	S_{BET} ($m^2\ g^{-1}$)	$S_{Langmuir}$ ($m^2\ g^{-1}$)	Total pore volume ($mm^3\ g^{-1}$)
CNTW_PP	94	100	247
CNTW_HDPE	75	78	184
CNTW_LDPE	66	68	172
CNT_PP	98	109	244
CNT_HDPE	80	89	215
CNT_LDPE	67	76	154
IO@Al_2O_3	139	160	326
GO	7	7	14
Al_2O_3	185	201	437

It is possible to see that the S_{BET} of the CNTs were not high if compared, for example, with some activated carbons (~1000 $m^2\ g^{-1}$ [161]) and carbon blacks (~178 $m^2\ g^{-1}$ [162]). Thereafter, the material CNTW_PP shows the highest S_{BET}, which can be explained by the different kind of hydrocarbons generated during the pyrolysis. This fact enables different characteristics of the CNTs as well as the higher formation of amorphous carbons, contributing to the surface area [150].

The synthesized materials have similar S_{BET} values if compared with those found in the literature for CNTs produced from plastics, such as 76.3 and 100.5 $m^2\ g^{-1}$ (HDPE) [151,163], and 74.5 $m^2\ g^{-1}$ (PP) [164].

GO shows a very low S_{BET}, which can be an indicator of very ordered GO layers, since the S_{BET} for this kind of material have a high dependence on the worsening order of graphene layers [158]. On the other hand, IO@Al_2O_3 presents a high S_{BET}, being very close to the values found in literature [150]. This high S_{BET} can be attributed to the presence of Al_2O_3 since the material shows high values of S_{BET} when compared with the other materials analysed, as can be seen in Table 4. The decrease in the S_{BET} of Al_2O_3 in the IO@Al_2O_3 may be attributed to the filling of the porous of the material with the IO particles.

4.2 Adsorption of paracetamol

Paracetamol adsorption experiments were performed to assess the contribution of the materials adsorption capacity in the removal of paracetamol (PCM). The results obtained with each material can be observed in Figure 16.

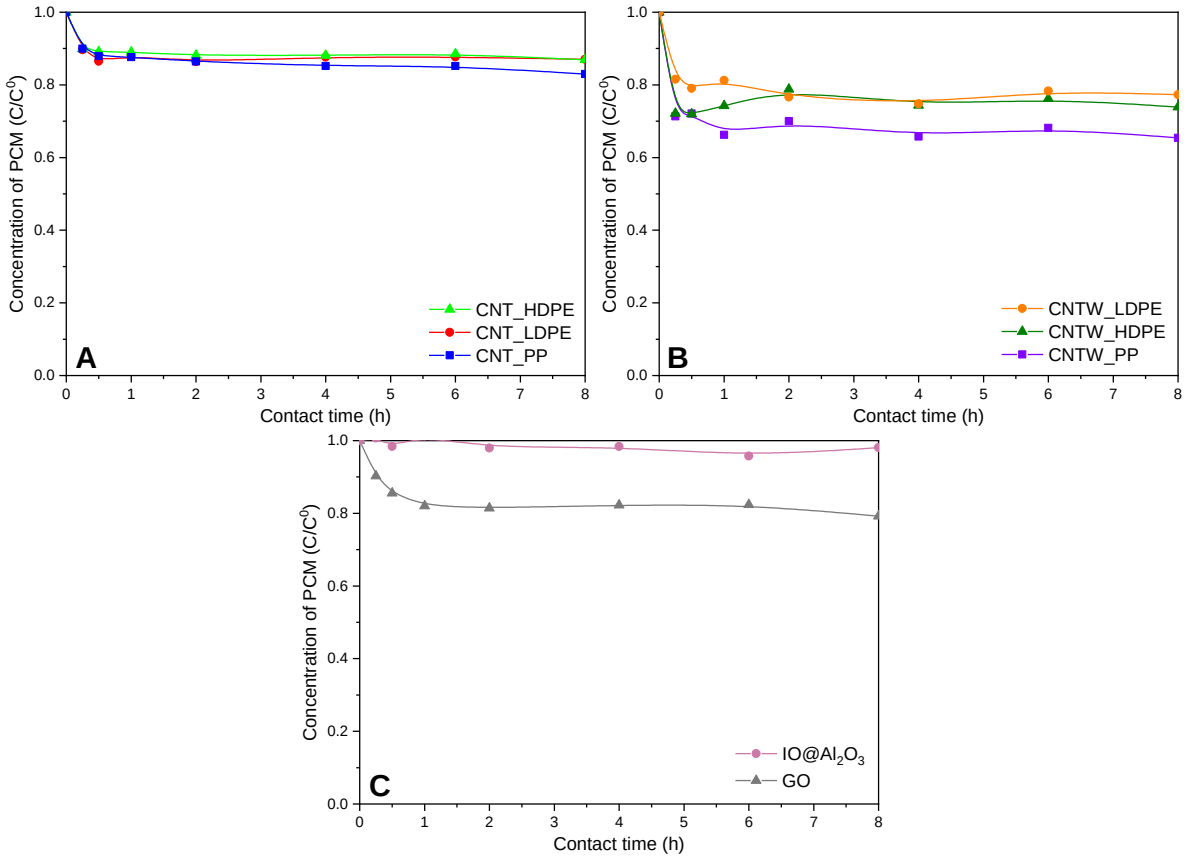

Figure 16 - PCM relative concentration during the adsorption test of A) CNTs, B) CNTWs, and C) other materials.

The adsorption curves show that the CNTW_PP is the material with highest adsorption, while IO@Al_2O_3 presents the lowest adsorption. The CNTs, shown in Figure 16

A, present a very close adsorption profile. However, it is possible to observe that the materials prepared from polyethylene present a profile more similar to the material produced from polypropylene, demonstrating the difference among the structure of the materials prepared from different carbon sources. The same can be observed among the CNTWs presented in Figure 16 Figure 16 - PCM relative concentration during the adsorption test of A) CNTs, B) CNTWs, and C) other materials.B, where this characteristic became even more evident. Between the CNTs and CNTWs, it is possible to conclude that the washing process increased the adsorption capacity of the materials, which can be explained by the removal of IO@Al_2O_3 in excess in the materials, since this material does not show high levels of adsorption, as can be observed in Figure 16 C. The material GO, also presented in Figure 16 C, presents low levels of adsorption, close to those found with the CNTs.

Comparing the CNTs and the CNTWs, the adsorption results are closely in line with the BET results (CNT_PP>CNT_LDPE>CNT_HDPE and CNTW_PP>CNTW_LDPE>CNTW_HDPE), where CNT_PP and CNTW_PP show higher adsorption capacity (15 and 35% of PCM concentration, respectively) than CNT_LDPE and CNTW_LDPE (12 and 23% of PCM concentration, respectively), and CNT_HDPE and CNTW_HDPE (11 and 26%, respectively) after 8 h of reaction. This result will further be compared with the CWPO to verify the proportion of PCM removed by adsorption and oxidation.

4.3 CWPO of paracetamol

The results of CWPO runs were evaluated taking into account each parameter evaluated i.e., PCM, H_2O_2, aromaticity, phenolic compounds and TOC.

4.3.1 PCM concentration

The evaluation of the concentration of PCM during the CWPO with each CNT as catalyst can be observed in Figure 17. The representation of the relative concentration profiles was shown in groups taking in account the materials as CNTs, CNTWs, non-catalyst and others.

Figure 17 A shows the removal of PCM using the non-washed CNTs prepared from LDPE, HDPE and PP. Even though all the CNTs degraded totally PCM in 2 h, among them it is possible to observe that the catalyst CNT_HDPE shows the highest catalytic activity, since PCM is degraded first (1 h). The order of catalytic activity among these materials follow the

same order of the ash content (CNT_HDPE>CNT_LDPE>CNT_PP), as given in Table 4, being the CNTs with higher amount of CVD-catalysts those presenting higher catalytic activity.

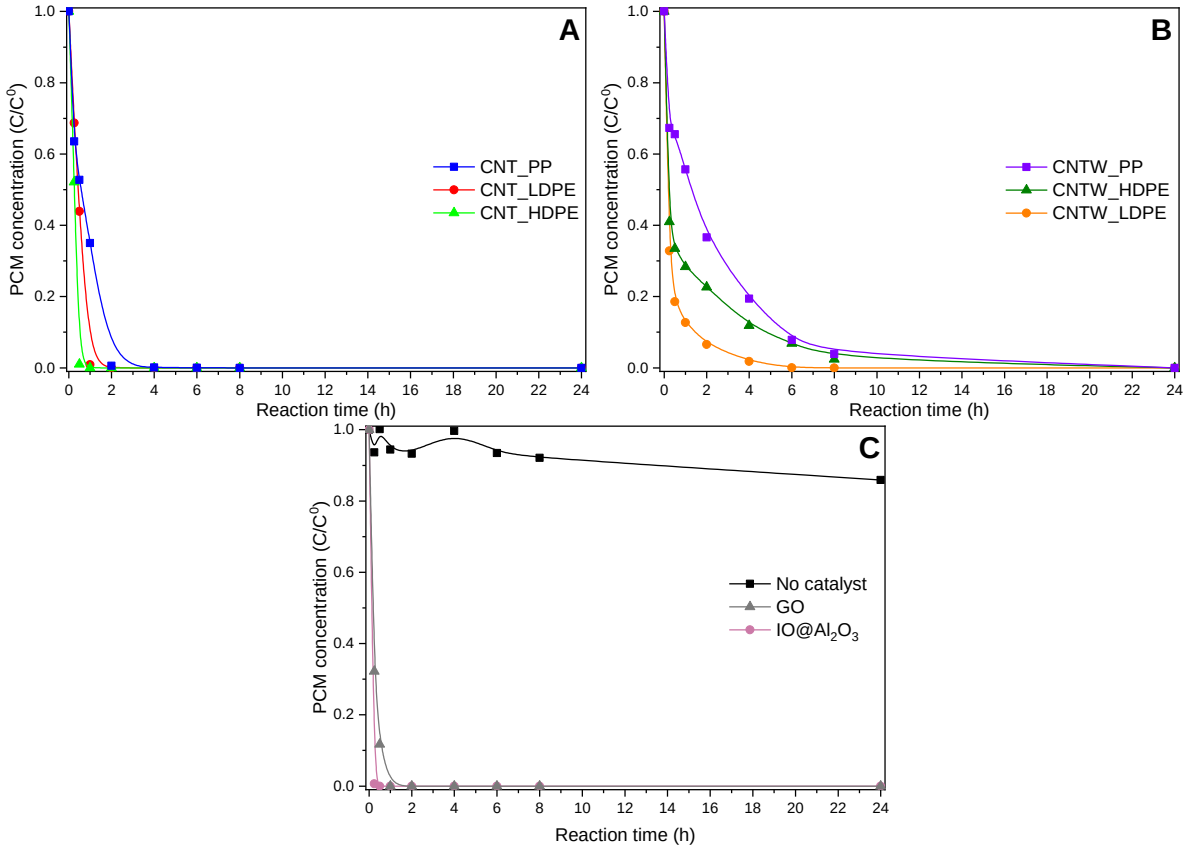

Figure 17 - Concentration of PCM during CWPO runs with A) CNTs, B) CNTWs, and C) other materials and no catalyst run.

The catalytic activity was found to be different among the washed CNTs (Figure 17 B) when compared to the CNTs before washing, the CNTW_LDPE being the most active in this series of materials, degrading all the pollutant after 6 h of reaction. CNTW_LDPE in this case presents the lowest catalysts content (ash content in Table 4). As previously explained in section 2.4, Fe plays a fundamental role in AOPs, thus the higher efficiency of CNTW_LDPE may be attributed to a possible higher presence of Fe in the structure of the CNTWs.

Figure 17 C shows the removal of PCM obtained with GO and IO@Al_2O_3 as catalysts and the wet peroxide oxidation of PCM without catalyst. As expected, pure IO@Al_2O_3 shows the highest catalytic activity, due to its higher presence of Fe when compared to the other catalysts. GO showed a relatively high catalytic activity considering the amount of metals in

the structure of this material, since it has lower ash content if compared with the CNTs, for example.

IO@Al_2O_3 shows the highest catalytic activity, followed by CNT_HDPE, GO, CNT_LDPE, CNT_PP, CNTW_LDPE, CNTW_HDPE and CNTW_PP. It is evident that the materials are efficient catalysts when compared with the non-catalytic run, indicating that the use of them contribute undoubtedly to the goal of the reaction.

Comparing the results found with others in literature that uses Fenton catalysts for oxidation of PCM, similar values are observed, such as 100% removal after 6h [165], 98.3% after 5.5h [166] and 100% after 5.5h [28]. Furthermore, compared to the studies shown in Table 2, the carbon nanostructures studied also show high catalytic activity in the removal of the micropollutant, since 100% of PCM was removed in all the CWPO runs.

Figure 18 compares the influence of adsorption in the PCM removal obtained by CWPO.

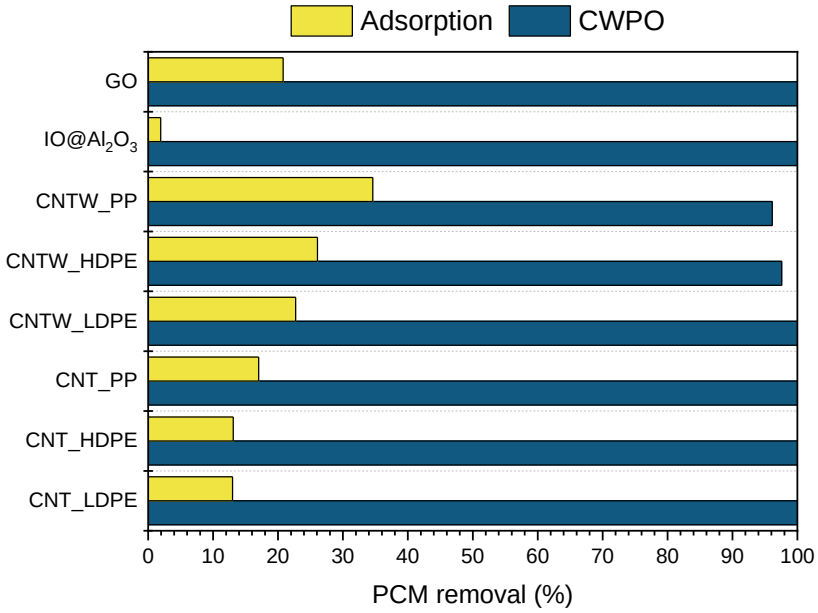

Figure 18 - Comparison between the removal of PCM by CWPO and pure adsorption.

It is possible to see that the CWPO promotes the PCM removal all the materials, probing that the pollutant was oxidized by the reaction and do not only by means of adsorption. It was more evident in the case of IO@Al_2O_3, mainly due to its low adsorption capacity. It also allows to see that the catalytic activity of the materials was high, demonstrating its potential for the targeted application. Among the CNTs, CNT_LDPE and CNT_HDPE show almost the same catalytic activity, demonstrating their similarity.

However, the CNTWs demonstrated a higher difference, where CNT_LDPE shows the best result of CWPO activity among them.

4.3.2 H_2O_2 concentration

The results of H_2O_2 decomposition against reaction time with each catalyst can be observed in Figure 19.

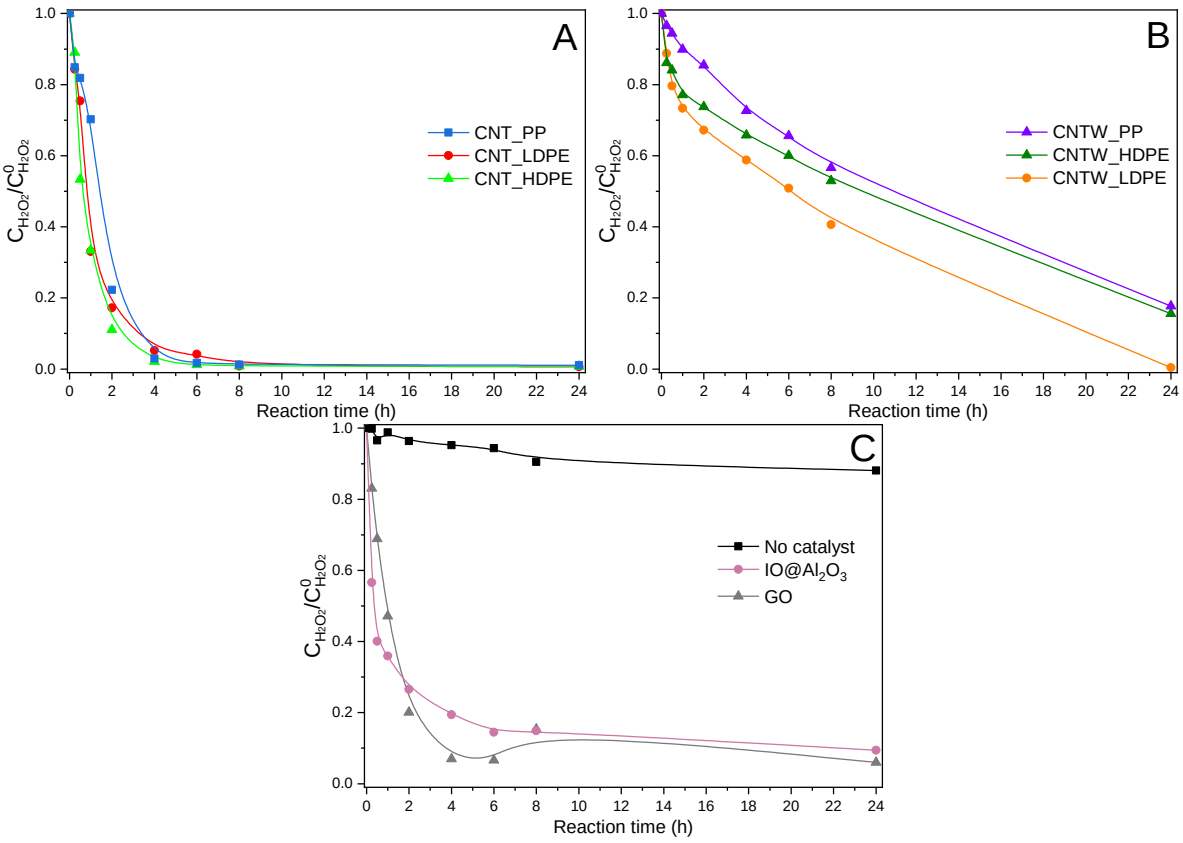

Figure 19 - Concentration of H_2O_2 during CWPO runs with A) CNTs, B) CNTWs, and C) other materials.

The profiles of H_2O_2 decomposition obtained with the non-washed CNTs as catalyst (Figure 19 A) are very similar and present a higher rate if compared with the CNTWs (Figure 19 B). This fact can be ascribed to the differences among the composition of these materials that promoted different H_2O_2 decompositions. The results obtained with the CNTWs support the results observed in the PCM profiles, where the material CNTW_LDPE become the most active CNT after the washing process. This result is in line with the possibility of a higher composition of Fe in the material CNTW_LDPE than in the other ones, since Fe increases the decomposition of H_2O_2 into $HO^{\bullet}$ radicals, which may explain the higher activity [54]. Figure 19 C shows the profiles obtained with GO and IO@Al_2O_3 as catalysts and the non-catalytic

reaction, showing that GO and IO@Al_2O_3 are not able to decompose all H_2O_2 present in the solution. This fact suggests that not only the presence of Fe in the catalyst is sufficient to promote the catalytic activity. Thus, the nanotubes are essential to promote a better decomposition of H_2O_2 and enable a more efficient process.

4.3.3 Aromatic compounds

The profiles of formation of aromatic compounds can be observed in Figure 20. In the oxidation of PCM there are many possible reaction routes. Thus, the most formed aromatic compounds in these reactions are hydroquinone, 4-aminophenol, 4-nitrophenol and catechol [28,167].

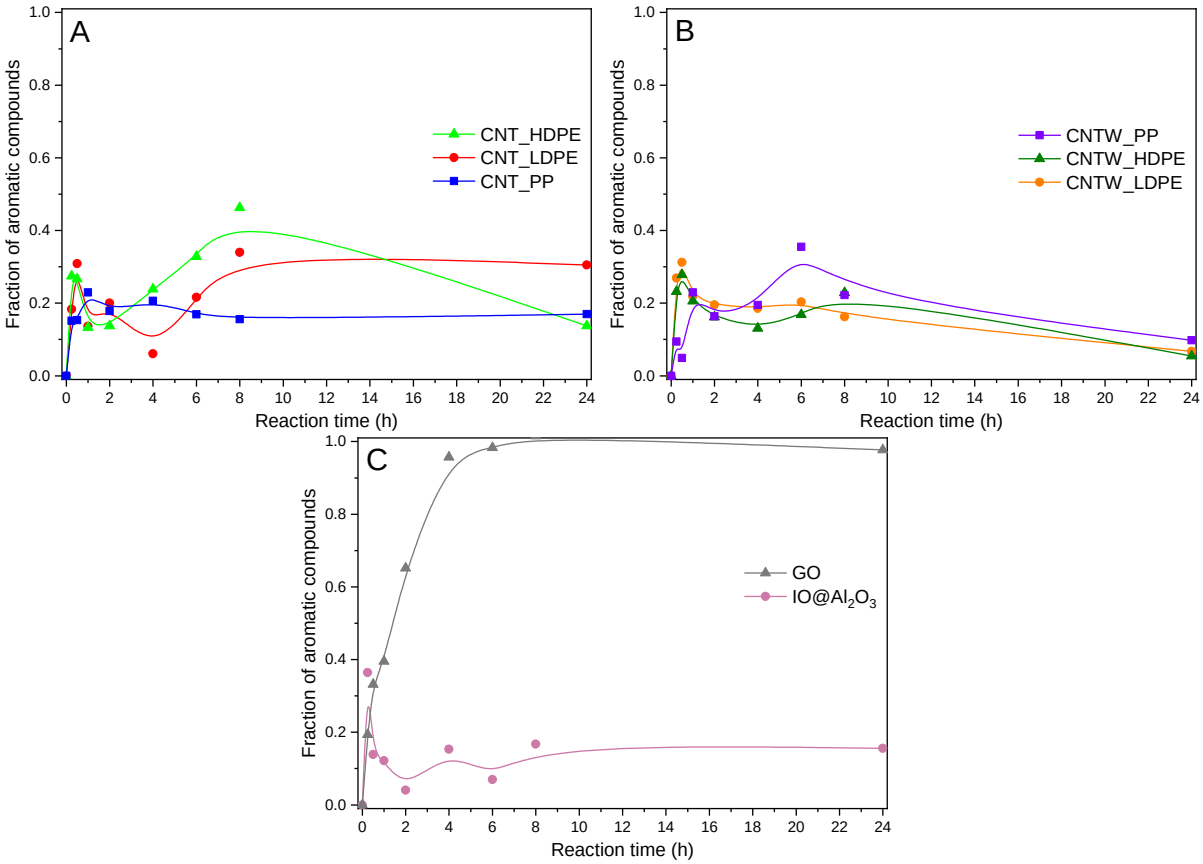

Figure 20 - Formation of aromatic compounds during CWPO runs with A) CNTs, B) CNTWs and C) other materials.

Figure 20 A shows the formation and further oxidation of aromatic compounds produced during the CWPO with the non-washed CNTs. In all CWPO runs aromatic compounds were produced, however, CNT_HDPE and CNT_PP were able to degrade the major part of the generated aromatic compounds, which was not observed with CNT_LDPE.

This can be justified by the possibility of different mechanisms of PCM degradation with each material since CNT_LDPE may have generated more refractory compounds than the other materials.

In the case of the CNTWs (Figure 20 B) all the materials show similar profiles, degrading almost all the aromatic compounds generated. The washed materials lead to the generation of lower amounts of aromatic compounds when compared with the non-washed materials, which also contributes to a lower formation of refractory compounds.

The other catalysts (Figure 20 C), show the presence of a huge amount of aromatic compounds in the case of GO, being not able to further degrade it. The discrepancy of this material could also be attributed to a different route of PCM degradation, where the great part of PCM may have been degraded into refractory aromatic compounds that GO were not able to decompose.

4.3.4 Phenolic compounds

The concentration profile of phenolic compounds, measured as milligrams of GA per litter, produced during the CWPO of paracetamol with washed catalysts is depicted in Figure 21. The tests of phenolic compounds were only done with non-washed materials to verify the capability of degradation of these materials.

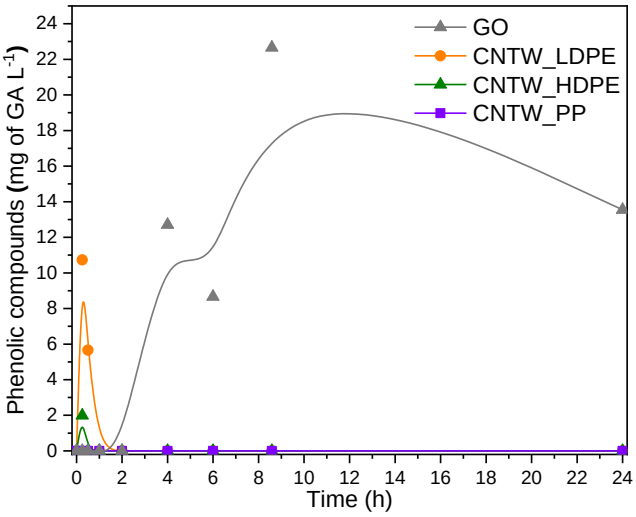

Figure 21 - Formation of phenolic compounds during the CWPO runs.

It is possible to observe that all the CNTWs were able to remove completely the phenolic compounds before 1 h, and the highest formation occurred between 0 and 30 min.

This result can be attributed to the degradation of PCM into phenolic intermediates such as p-aminophenol, hydroquinone, 4-nitrocatechol and 4-nitrophenol [167]. As expected, GO generated the highest amount of phenolic compounds, since this material also generated the highest amount of aromatic compounds as well. However, unlike the CNTWs, GO was not capable to degrade the generated phenolic compounds, resulting in the concentration of other compounds in the solution.

4.3.5 Identification of oxidized intermediates and products

There has been reported in the literature many possible pathways for the oxidation of PCM. The most reported pathways are the oxidation of PCM directly into hydroxyacetaminophen, 4-aminophenol, benzoquinone, hydroquinone, catechol, resorcinol or 4-nitrocatechol [167,168]. From that, many other reactional routes can occur, leading to the formation of pyrogallol, nitrophenol, 4-nitrophenol and carboxylic acids [167]. Thus, depending the reactional conditions, different mechanisms are possible.

Using the results of the HPLC tests, it was possible to detect some intermediates formed in the reactions. In the case of GO, the aromatic and phenolic compounds that were not degraded can be mainly composed by 4-nitrocatechol, since this substance was the only one detected by the methodology used in the HPLC, and was found from 2 h and kept present until 24 h.

The reaction run carried out with CNTW_LDPE presented the formation of hydroquinone, catechol, phenol and 4-nitrocatechol after 15 min, hydroquinone after 30 min, 4-nitrocatechol after 1 h, pyrogallol after 2 h, and pyrogallol and benzoquinone after 4 h. Then, after 6 h there was no more intermediates found. The higher formation of intermediates in the first 15 min of the reaction can explain the results of aromatic and phenolic compounds indicated in the previous tests, since they have shown the highest levels of these components around this time of reaction. Besides that, these components generate higher concentrations of these intermediates if compared with the other materials.

In the case of the reaction run carried out with CNTW_HDPE, compounds such as hydroquinone, catechol and 4-nitrocatechol were formed after 15 min, and hydroquinone until 6 h of reaction. After 8 h no more intermediates were formed. The formation of these compounds agrees with those found in the aromatic and phenolic tests, since CNTW_HDPE had its highest formation of intermediates around 15 min.

In the of the reaction run carried out with CNTW_PP, the formation of hydroquinone was observed between 2 and 8 h of reaction, presenting no intermediates before and after those times. This result agrees with the aromatic test, since CNTW_PP had its highest formation of intermediates around 6 h. However, the phenolic test could not detect this substance. This fact can be due to the lower concentration found for hydroquinone in the reaction, if compared with the other components in the reaction.

4.3.6 Reusability

The catalyst chosen for the reusability tests was the CNTW_LDPE since it is the material with a relative low Fe content that presented high catalytic activity. Thus, 3 runs were performed with this material and evaluated the first and the third runs, as shown in Figure 22.

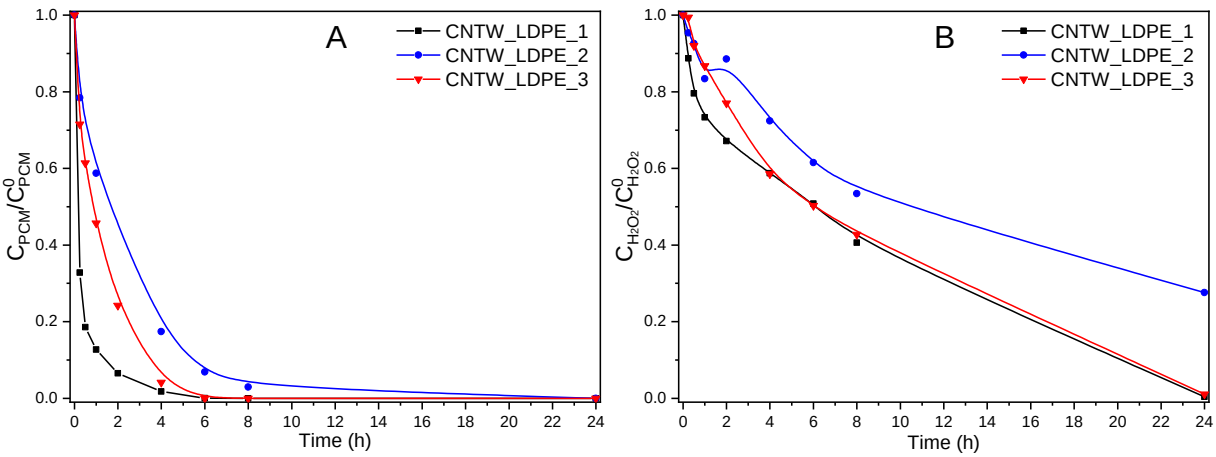

Figure 22 - Reusability capacity of CNTW_LDPE in terms of A) PCM concentration and B) H_2O_2 concentration.

As can be observed, after 3 runs the catalyst kept a great part of its catalytic activity, mainly in H_2O_2 decomposition. This fact can indicate that the material has a good structure stability, which is in favor of the viability of the catalyst. The high level of H_2O_2 decomposition, even after using the catalyst 3 times, also indicates that morphological, structural and interactions among Fe, Al and carbon content remained in the catalyst.

CONCLUSIONS

5 CONCLUSIONS

The synthesis of IO@Al_2O_3 further used as CVD-catalyst was done by the sol-gel method, obtaining a red-brown catalyst. The use of this CVD-catalyst led to produce magnetic CNTs. The washing process could remove the great part of the remaining IO@Al_2O_3 from the structure of the CNT materials, proved by the ash content between the washed and non-washed CNTs.

The conducted treatment of a water contaminated with paracetamol by CWPO was successful for all the CNTs used as catalysts, since all of them could degrade 100% of the pollutant until 1440 min. Then the catalysts were efficient in the degradation of PCM by CWPO when compared to the CWPO run conducted without catalyst. The CNT with the lower Fe content and the highest relative activity was the CNTW_LDPE, demonstrating the capacity to degrade all the pollutant (PCM and some intermediates followed as aromatics and total phenols) after 360 min. This catalyst was tested to verify its reusability, and it showed that the catalyst kept the catalytic activity after 3 runs.

Since the catalyst obtained from carbon sources showed high PCM degradation, it contributes to possible valorization of carbon wastes and its use for micropollutant removal as promise technology for water quality improvement.

As suggestions for future works, other polymers may be tested in the CVD for CNTs synthesis, removal of other pollutants, and further analysis of the conducted CWPO, such as TOC.

REFERENCES

6 REFERENCES

[1] United States Environmental Protection Agency, AQUATIC LIFE CRITERIA FOR CONTAMINANTS OF EMERGING CONCERN - GENERAL CHALLENGES AND RECOMMENDATIONS, United States of America, 2008.

[2] Water Quality Association, Contaminants of Emerging Concern, (n.d.). https://www.wqa.org/whats-in-your-water/emerging-contaminants (accessed July 22, 2020).

[3] U. S. Geological Survey, Contaminants of Emerging Concern in the Environment, (2017). https://toxics.usgs.gov/investigations/cec/index.php (accessed July 22, 2020).

[4] U. S. Geological Survey, Emerging Contaminants, (n.d.). https://www.usgs.gov/mission-areas/water-resources/science/emerging-contaminants?qt-science_center_objects=0#qt-science_center_objects (accessed July 22, 2020).

[5] L.M. Madikizela, S. Ncube, L. Chimuka, Analysis, occurrence and removal of pharmaceuticals in African water resources: A current status, J. Environ. Manage. 253 (2020) 109741. https://doi.org/10.1016/j.jenvman.2019.109741.

[6] B. Hong, S. Yu, Y. Niu, J. Ding, Q. Lin, X. Lin, W. Hu, Spectrum and environmental risks of residual pharmaceuticals in stream water with emphasis on its relation to epidemic infectious disease and anthropogenic activity in watershed, J. Hazard. Mater. 385 (2020) 121594. https://doi.org/10.1016/j.jhazmat.2019.121594.

[7] D. Pemberthy M, Y. Padilla, A. Echeverri, G.A. Peñuela, Monitoring pharmaceuticals and personal care products in water and fish from the Gulf of Urabá, Colombia, Heliyon. 6 (2020). https://doi.org/10.1016/j.heliyon.2020.e04215.

[8] L. Niemi, M. Taggart, K. Boyd, Z. Zhang, P.P.J. Gaffney, S. Pfleger, S. Gibb, Assessing hospital impact on pharmaceutical levels in a rural 'source-to-sink' water system, Sci. Total Environ. 737 (2020). https://doi.org/10.1016/j.scitotenv.2020.139618.

[9] C.F. Couto, L.C. Lange, M.C.S. Amaral, Occurrence, fate and removal of pharmaceutically active compounds (PhACs) in water and wastewater treatment plants—A review, J. Water Process Eng. 32 (2019) 100927. https://doi.org/10.1016/j.jwpe.2019.100927.

[10] S.M. Praveena, M.Z. Mohd Rashid, F.A. Mohd Nasir, W. Sze Yee, A.Z. Aris, Occurrence and potential human health risk of pharmaceutical residues in drinking

water from Putrajaya (Malaysia), Ecotoxicol. Environ. Saf. 180 (2019) 549–556. https://doi.org/10.1016/j.ecoenv.2019.05.051.

[11] Y. Song, Y. Ding, F. Wang, Y. Chen, Y. Jiang, Construction of nano-composites by enzyme entrapped in mesoporous dendritic silica particles for efficient biocatalytic degradation of antibiotics in wastewater, Chem. Eng. J. 375 (2019) 121968. https://doi.org/10.1016/j.cej.2019.121968.

[12] M.T. Pinho, H.T. Gomes, R.S. Ribeiro, J.L. Faria, A.M.T. Silva, Carbon nanotubes as catalysts for catalytic wet peroxide oxidation of highly concentrated phenol solutions: Towards process intensification, Appl. Catal. B Environ. 165 (2015) 706–714. https://doi.org/10.1016/j.apcatb.2014.10.057.

[13] M.R. Barati, M. Aghbashlo, H. Ghanavati, M. Tabatabaei, M. Sharifi, G. Javadirad, A. Dadak, M. Mojarab Soufiyan, Comprehensive exergy analysis of a gas engine-equipped anaerobic digestion plant producing electricity and biofertilizer from organic fraction of municipal solid waste, Energy Convers. Manag. 151 (2017) 753–763. https://doi.org/10.1016/j.enconman.2017.09.017.

[14] M. Aghbashlo, M. Tabatabaei, S. Soltanian, H. Ghanavati, Biopower and biofertilizer production from organic municipal solid waste: An exergoenvironmental analysis, Renew. Energy. 143 (2019) 64–76. https://doi.org/10.1016/j.renene.2019.04.109.

[15] N. Torbick, S. Hession, S. Hagen, N. Wiangwang, B. Becker, J. Qi, Mapping inland lake water quality across the Lower Peninsula of Michigan using Landsat TM imagery, Int. J. Remote Sens. 34 (2013) 7607–7624. https://doi.org/10.1080/01431161.2013.822602.

[16] A. Gil, L.A. Galeano, M.À. Vicente, Applications of Advanced Oxidation Processes (AOPs) in Drinking Water Treatment, Springer International Publishing, 2019. https://doi.org/10.1007/978-3-319-76882-3.

[17] World Health Organization, Drinking-water, (2019). https://www.who.int/en/news-room/fact-sheets/detail/drinking-water (accessed May 16, 2020).

[18] S. Bagnis, A. Boxall, A. Gachanja, M. Fitzsimons, M. Murigi, J. Snape, A. Tappin, J. Wilkinson, S. Comber, Characterization of the Nairobi River catchment impact zone and occurrence of pharmaceuticals: Implications for an impact zone inclusive environmental risk assessment, Sci. Total Environ. 703 (2020) 134925. https://doi.org/10.1016/j.scitotenv.2019.134925.

[19] EEB - The European Environmental Bureau, The problem of pharmaceutical pollution, (n.d.). https://eeb.org/the-problem-of-pharmaceutical-pollution/ (accessed May 17,

2020).

[20] R.R. Singh, L.F. Angeles, D.M. Butryn, J.W. Metch, E. Garner, P.J. Vikesland, D.S. Aga, Towards a harmonized method for the global reconnaissance of multi-class antimicrobials and other pharmaceuticals in wastewater and receiving surface waters, Environ. Int. 124 (2019) 361–369. https://doi.org/10.1016/j.envint.2019.01.025.

[21] K. He, A.G. Borthwick, Y. Lin, Y. Li, J. Fu, Y. Wong, W. Liu, Sale-based estimation of pharmaceutical concentrations and associated environmental risk in the Japanese wastewater system, Environ. Int. 139 (2020) 105690. https://doi.org/10.1016/j.envint.2020.105690.

[22] P.A. Segura, M. François, C. Gagnon, S. Sauvé, Review of the occurrence of anti-infectives in contaminated wastewaters and natural and drinking waters, Environ. Health Perspect. 117 (2009) 675–684. https://doi.org/10.1289/ehp.11776.

[23] E. Corsini, E. Sangiovanni, A. Avogadro, V. Galbiati, B. Viviani, M. Marinovich, C.L. Galli, M. Dell'Agli, D.R. Germolec, In vitro characterization of the immunotoxic potential of several perfluorinated compounds (PFCs), Toxicol. Appl. Pharmacol. 258 (2012) 248–255. https://doi.org/10.1016/j.taap.2011.11.004.

[24] S. Suárez, M. Carballa, F. Omil, J.M. Lema, How are pharmaceutical and personal care products (PPCPs) removed from urban wastewaters?, Rev. Environ. Sci. Biotechnol. 7 (2008) 125–138. https://doi.org/10.1007/s11157-008-9130-2.

[25] S. Zhou, C. Di Paolo, X. Wu, Y. Shao, T.B. Seiler, H. Hollert, Optimization of screening-level risk assessment and priority selection of emerging pollutants – The case of pharmaceuticals in European surface waters, Environ. Int. 128 (2019) 1–10. https://doi.org/10.1016/j.envint.2019.04.034.

[26] Z. Tousova, P. Oswald, J. Slobodnik, L. Blaha, M. Muz, M. Hu, W. Brack, M. Krauss, C. Di Paolo, Z. Tarcai, T.B. Seiler, H. Hollert, S. Koprivica, M. Ahel, J.E. Schollée, J. Hollender, M.J.F. Suter, A.O. Hidasi, K. Schirmer, M. Sonavane, S. Ait-Aissa, N. Creusot, F. Brion, J. Froment, A.C. Almeida, K. Thomas, K.E. Tollefsen, S. Tufi, X. Ouyang, P. Leonards, M. Lamoree, V.O. Torrens, A. Kolkman, M. Schriks, P. Spirhanzlova, A. Tindall, T. Schulze, European demonstration program on the effect-based and chemical identification and monitoring of organic pollutants in European surface waters, Sci. Total Environ. 601–602 (2017) 1849–1868. https://doi.org/10.1016/j.scitotenv.2017.06.032.

[27] EUR-Lex - 32015D0495 - EN - EUR-Lex, (n.d.). https://eur-lex.europa.eu/eli/dec_impl/2015/495/oj (accessed May 18, 2020).

[28] F. Velichkova, H. Delmas, C. Julcour, B. Koumanova, Heterogeneous fenton and photo-fenton oxidation for paracetamol removal using iron containing ZSM-5 zeolite as catalyst, AIChE J. 63 (2017) 669–679. https://doi.org/10.1002/aic.15369.

[29] M.Á. López Zavala, C.R. Jaber Lara, Degradation of paracetamol and its oxidation products in surface water by electrochemical oxidation, Environ. Eng. Sci. 35 (2018) 1248–1254. https://doi.org/10.1089/ees.2018.0023.

[30] CONAMA, Resolução N° 430, De 13 De Maio De 2011, http://www2.mma.gov.br/port/conama/processo.cfm?processo=02000.001876/2008-64, Brazil, 2011. http://www.mma.gov.br/port/conama/legiabre.cfm?codlegi=646.

[31] Ministério do Ambiente, Decreto Lei nº 236/98, 1998.

[32] European Parliament, COUNCIL DIRECTIVE of 21 May 1991; concerning urban waste water treatment, 1991.

[33] A.J. Englande, P. Krenkel, J. Shamas, Wastewater Treatment &Water Reclamation, Elsevier Inc., 2015. https://doi.org/10.1016/b978-0-12-409548-9.09508-7.

[34] F.Y. Wang, V. Rudolph, Z.H. Zhu, Sewage Sludge Technologies, Encycl. Ecol. Five-Volume Set. i (2008) 3227–3242. https://doi.org/10.1016/B978-008045405-4.00078-1.

[35] F.R. Spellman, Wastewater Treatment Operations, CRC Press, 2013. https://doi.org/10.1201/b15579-27.

[36] G. Kooijman, M.K. de Kreuk, C. Houtman, J.B. van Lier, Perspectives of coagulation/flocculation for the removal of pharmaceuticals from domestic wastewater: A critical view at experimental procedures, J. Water Process Eng. 34 (2020) 101161. https://doi.org/10.1016/j.jwpe.2020.101161.

[37] T.A. Ternes, M. Meisenheimer, D. McDowell, F. Sacher, H.J. Brauch, B. Haist-Gulde, G. Preuss, U. Wilme, N. Zulei-Seibert, Removal of pharmaceuticals during drinking water treatment, Environ. Sci. Technol. 36 (2002) 3855–3863. https://doi.org/10.1021/es015757k.

[38] M. Carballa, F. Omil, J.M. Lema, Removal of cosmetic ingredients and pharmaceuticals in sewage primary treatment, Water Res. 39 (2005) 4790–4796. https://doi.org/10.1016/j.watres.2005.09.018.

[39] V. de Jesus Gaffney, V.V. Cardoso, E. Cardoso, A.P. Teixeira, J. Martins, M.J. Benoliel, C.M.M. Almeida, Occurrence and behaviour of pharmaceutical compounds in a Portuguese wastewater treatment plant: Removal efficiency through conventional treatment processes, Environ. Sci. Pollut. Res. 24 (2017) 14717–14734. https://doi.org/10.1007/s11356-017-9012-7.

[40] R. Loos, R. Carvalho, D.C. António, S. Comero, G. Locoro, S. Tavazzi, B. Paracchini, M. Ghiani, T. Lettieri, L. Blaha, B. Jarosova, S. Voorspoels, K. Servaes, P. Haglund, J. Fick, R.H. Lindberg, D. Schwesig, B.M. Gawlik, EU-wide monitoring survey on emerging polar organic contaminants in wastewater treatment plant effluents, Water Res. 47 (2013) 6475–6487. https://doi.org/10.1016/j.watres.2013.08.024.

[41] S.D. Kim, J. Cho, I.S. Kim, B.J. Vanderford, S.A. Snyder, Occurrence and removal of pharmaceuticals and endocrine disruptors in South Korean surface, drinking, and waste waters, Water Res. 41 (2007) 1013–1021. https://doi.org/10.1016/j.watres.2006.06.034.

[42] S. Wu, L. Zhang, J. Chen, Paracetamol in the environment and its degradation by microorganisms, Appl. Microbiol. Biotechnol. 96 (2012) 875–884. https://doi.org/10.1007/s00253-012-4414-4.

[43] I. Kim, N. Yamashita, H. Tanaka, Performance of UV and UV/H_2O_2 processes for the removal of pharmaceuticals detected in secondary effluent of a sewage treatment plant in Japan, J. Hazard. Mater. 166 (2009) 1134–1140. https://doi.org/10.1016/j.jhazmat.2008.12.020.

[44] A.J. Ebele, T. Oluseyi, D.S. Drage, S. Harrad, M. Abou-Elwafa Abdallah, Occurrence, seasonal variation and human exposure to pharmaceuticals and personal care products in surface water, groundwater and drinking water in Lagos State, Nigeria, Emerg. Contam. 6 (2020) 124–132. https://doi.org/10.1016/j.emcon.2020.02.004.

[45] A.Z. Tong, A.J. Ghoshdastidar, S. Fox, The presence of the top prescribed pharmaceuticals in treated sewage effluents and receiving waters in southwest nova scotia, canada, Environ. Sci. Pollut. Res. 22 (2015) 689–700. https://doi.org/10.1007/s11356-014-3400-z.

[46] X. Tong, Z. Li, W. Chen, J. Wang, X. Li, J. Mu, Y. Tang, L. Li, Efficient catalytic ozonation of diclofenac by three-dimensional iron (Fe)-doped SBA-16 mesoporous structures, J. Colloid Interface Sci. 578 (2020) 461–470. https://doi.org/10.1016/j.jcis.2020.06.003.

[47] J.L. Diaz de Tuesta, B. F. Machado, P. Serp, A.M. Adrián, J.L. Faria, H. T. Gomes, Janus amphiphilic carbon nanotubes as Pickering interfacial catalysts for the treatment of oily wastewater by selective oxidation with hydrogen peroxide, Catal. Today. (2019) 1–11. https://doi.org/10.1016/j.cattod.2019.07.012.

[48] S.A. Parsons, Advanced oxidation processes for water/wastewater treatment, IWA, London, 2004. https://doi.org/https://doi.org/10.2166/9781780403076.

[49] E. Brillas, A review on the photoelectro-Fenton process as efficient electrochemical advanced oxidation for wastewater remediation. Treatment with UV light, sunlight, and coupling with conventional and other photo-assisted advanced technologies, Chemosphere. 250 (2020) 126198. https://doi.org/10.1016/j.chemosphere.2020.126198.

[50] A.H. Khan, N.A. Khan, S. Ahmed, A. Dhingra, C.P. Singh, S.U. Khan, A.A. Mohammadi, F. Changani, M. Yousefi, S. Alam, S. Vambol, V. Vambol, A. Khursheed, I. Ali, Application of advanced oxidation processes followed by different treatment technologies for hospital wastewater treatment, J. Clean. Prod. 269 (2020). https://doi.org/10.1016/j.jclepro.2020.122411.

[51] J. Wang, R. Zhuan, Degradation of antibiotics by advanced oxidation processes: An overview, Sci. Total Environ. 701 (2020) 135023. https://doi.org/10.1016/j.scitotenv.2019.135023.

[52] S. Arzate, S. Pfister, C. Oberschelp, J.A. Sánchez-Pérez, Environmental impacts of an advanced oxidation process as tertiary treatment in a wastewater treatment plant, Sci. Total Environ. 694 (2019). https://doi.org/10.1016/j.scitotenv.2019.07.378.

[53] Y. Deng, R. Zhao, Advanced Oxidation Processes (AOPs) in Wastewater Treatment, Curr. Pollut. Reports. 1 (2015) 167–176. https://doi.org/10.1007/s40726-015-0015-z.

[54] A. Matilainen, M. Sillanpää, Removal of natural organic matter from drinking water by advanced oxidation processes, Chemosphere. 80 (2010) 351–365. https://doi.org/10.1016/j.chemosphere.2010.04.067.

[55] W.H. Glaze, J.W. Kang, D.H. Chapin, The chemistry of water treatment processes involving ozone, hydrogen peroxide and ultraviolet radiation, Ozone Sci. Eng. 9 (1987) 335–352. https://doi.org/10.1080/01919518708552148.

[56] H. Suty, C. De Traversay, M. Cost, Applications of advanced oxidation processes : present and future, Water Sci. Technol. 49 (2000) 227–233. https://doi.org/10.2166/wst.2004.0270.

[57] S. Chaliha, K.G. Bhattacharyya, Using Mn(II)- MCM41 as an environment-friendly catalyst to oxidize phenol, 2-chlorophenol, and 2-nitrophenol in aqueous solution, Ind. Eng. Chem. Res. 47 (2008) 1370–1379. https://doi.org/10.1021/ie071075f.

[58] W.J. Cooper, S. a. Snyder, S.P. Mezyk, J.R. Peller, M.G. Nickelsen, Reaction Rates and Mechanisms of Advanced Oxidation Processes (AOPs) for Water Reuse, WateReuse Foundation, 2010.

[59] P. V. Gayathri, S. Yesodharan, E.P. Yesodharan, Microwave/Persulphate assisted ZnO

mediated photocatalysis (MW/PS/UV/ZnO) as an efficient advanced oxidation process for the removal of RhB dye pollutant from water, J. Environ. Chem. Eng. 7 (2019) 103122. https://doi.org/10.1016/j.jece.2019.103122.

[60] M. hui Zhang, H. Dong, L. Zhao, D. xi Wang, D. Meng, A review on Fenton process for organic wastewater treatment based on optimization perspective, Sci. Total Environ. 670 (2019) 110–121. https://doi.org/10.1016/j.scitotenv.2019.03.180.

[61] A. Fernandes, C. Pereira, V. Kozioł, M.J. Pacheco, L. Ciríaco, A. Lopes, Emerging contaminants removal from effluents with complex matrices by electrooxidation, Sci. Total Environ. 740 (2020). https://doi.org/10.1016/j.scitotenv.2020.140153.

[62] H.A. Aziz, S.S.A. Amr, Advanced Oxidation Processes (AOPs) in Water and Wastewater Treatment, IGI Global, 2019.

[63] C. Lee, J. Yoon, U. Von Gunten, Oxidative degradation of N-nitrosodimethylamine by conventional ozonation and the advanced oxidation process ozone/hydrogen peroxide, Water Res. 41 (2007) 581–590. https://doi.org/10.1016/j.watres.2006.10.033.

[64] J.L. Acero, U. Von Gunten, Characterization of oxidation processes: Ozonation and the AOP O_3/H_2O_2, J. Am. Water Work. Assoc. 93 (2001) 90–100. https://doi.org/10.1002/j.1551-8833.2001.tb09311.x.

[65] S. Navalon, M. Alvaro, H. Garcia, Heterogeneous Fenton catalysts based on clays, silicas and zeolites, Appl. Catal. B Environ. 99 (2010) 1–26. https://doi.org/10.1016/j.apcatb.2010.07.006.

[66] G.P. Anipsitakis, D.D. Dionysiou, Radical generation by the interaction of transition metals with common oxidants, Environ. Sci. Technol. 38 (2004) 3705–3712. https://doi.org/10.1021/es035121o.

[67] H. Kušić, N. Koprivanac, A.L. Božić, I. Selanec, Photo-assisted Fenton type processes for the degradation of phenol: A kinetic study, J. Hazard. Mater. 136 (2006) 632–644. https://doi.org/10.1016/j.jhazmat.2005.12.046.

[68] N.S. Inchaurrondo, P. Massa, R. Fenoglio, J. Font, P. Haure, Efficient catalytic wet peroxide oxidation of phenol at moderate temperature using a high-load supported copper catalyst, Chem. Eng. J. 198–199 (2012) 426–434. https://doi.org/10.1016/j.cej.2012.05.103.

[69] M.I. Badawy, R.A. Wahaab, Fenton-biological treatment processes for the removal of some pharmaceuticals from industrial wastewater, J. Hazard. Mater. 167 (2009) 567–574. https://doi.org/10.1016/j.jhazmat.2009.01.023.

[70] A. Mirzaei, Z. Chen, F. Haghighat, L. Yerushalmi, Removal of pharmaceuticals from

water by homo / heterogonous Fenton-type processes e A review, Chemosphere. 174 (2017) 665–688. https://doi.org/10.1016/j.chemosphere.2017.02.019.

[71] Y. Yan, S. Jiang, H. Zhang, Efficient catalytic wet peroxide oxidation of phenol over Fe-ZSM-5 catalyst in a fixed bed reactor, Sep. Purif. Technol. 133 (2014) 365–374. https://doi.org/10.1016/j.seppur.2014.07.014.

[72] Y. Wu, H. Zhang, Y. Yan, Effect of copper ion-exchange on catalytic wet peroxide oxidation of phenol over ZSM-5 membrane, J. Environ. Manage. 270 (2020) 110907. https://doi.org/10.1016/j.jenvman.2020.110907.

[73] Z. Li, F. Liu, Y. Ding, F. Wang, H. You, C. Jin, Preparation and properties of Cu-Ni bimetallic oxide catalyst supported on activated carbon for microwave assisted catalytic wet hydrogen peroxide oxidation for biologically pretreated coal chemical industry wastewater treatment, Chemosphere. 214 (2019) 17–24. https://doi.org/10.1016/j.chemosphere.2018.09.098.

[74] M. Kurian, D.S. Nair, On the efficiency of cobalt zinc ferrite nanoparticles for catalytic wet peroxide oxidation of 4-chlorophenol, J. Environ. Chem. Eng. 2 (2014) 63–69. https://doi.org/10.1016/j.jece.2013.11.026.

[75] L.A. Galeano, M.Á. Vicente, A. Gil, Treatment of municipal leachate of landfill by fenton-like heterogeneous catalytic wet peroxide oxidation using an Al/Fe-pillared montmorillonite as active catalyst, Chem. Eng. J. 178 (2011) 146–153. https://doi.org/10.1016/j.cej.2011.10.031.

[76] D.S. Nair, M. Kurian, Catalytic peroxide oxidation of persistent chlorinated organics over nickel-zinc ferrite nanocomposites, J. Water Process Eng. 16 (2017) 69–80. https://doi.org/10.1016/j.jwpe.2016.12.010.

[77] X. Ou, F. Pilitsis, Y. Jiao, Y. Zhang, S. Xu, M. Jennings, Y. Yang, S.F.R. Taylor, A. Garforth, H. Zhang, C. Hardacre, Y. Yan, X. Fan, Hierarchical Fe-ZSM-5/SiC foam catalyst as the foam bed catalytic reactor (FBCR) for catalytic wet peroxide oxidation (CWPO), Chem. Eng. J. 362 (2019) 53–62. https://doi.org/10.1016/j.cej.2019.01.019.

[78] R. Ben Achma, A. Ghorbel, A. Dafinov, F. Medina, Copper-supported pillared clay catalysts for the wet hydrogen peroxide catalytic oxidation of model pollutant tyrosol, Appl. Catal. A Gen. 349 (2008) 20–28. https://doi.org/10.1016/j.apcata.2008.07.021.

[79] C.S.D. Rodrigues, S.A.C. Carabineiro, F.J. Maldonado-Hódar, L.M. Madeira, Wet peroxide oxidation of dye-containing wastewaters using nanosized Au supported on Al_2O_3, Catal. Today. 280 (2017) 165–175. https://doi.org/10.1016/j.cattod.2016.06.031.

[80] H. Qin, R. Xiao, J. Chen, Catalytic wet peroxide oxidation of benzoic acid over Fe/AC catalysts: Effect of nitrogen and sulfur co-doped activated carbon, Sci. Total Environ. 626 (2018) 1414–1420. https://doi.org/10.1016/j.scitotenv.2018.01.206.

[81] L. Singh, P. Rekha, S. Chand, Comparative evaluation of synthesis routes of Cu/zeolite Y catalysts for catalytic wet peroxide oxidation of quinoline in fixed-bed reactor, J. Environ. Manage. 215 (2018) 1–12. https://doi.org/10.1016/j.jenvman.2018.03.021.

[82] J.J.R. Márquez, I. Levchuk, M. Sillanpää, Application of catalytic wet peroxide oxidation for industrial and urban wastewater treatment: A review, Catalysts. 8 (2018). https://doi.org/10.3390/catal8120673.

[83] Z.M. De Pedro, M. Munoz, J. Nieto-sandoval, S. Cir, A. Quesada, J.A. Casas, Degradation of widespread cyanotoxins with high impact in drinking water (microcystins , cylindrospermopsin , anatoxin- a and saxitoxin) by CWPO, Water Res. 163 (2019). https://doi.org/10.1016/j.watres.2019.114853.

[84] J.L. Diaz de Tuesta, A. Quintanilla, D. Moreno, V.R. Ferro, J.A. Casas, Simulation and optimization of the CWPO process by combination of aspen plus and 6-factor doehlert matrix: Towards autothermal operation, Catalysts. 10 (2020). https://doi.org/10.3390/catal10050548.

[85] G. Pliego, J.A. Zazo, S. Blasco, J.A. Casas, J.J. Rodriguez, Treatment of highly polluted hazardous industrial wastewaters by combined coagulation - Adsorption and high-temperature fenton oxidation, Ind. Eng. Chem. Res. 51 (2012) 2888–2896. https://doi.org/10.1021/ie202587b.

[86] P. Cañizares, R. Paz, C. Sáez, M.A. Rodrigo, Costs of the electrochemical oxidation of wastewaters: A comparison with ozonation and Fenton oxidation processes, J. Environ. Manage. 90 (2009) 410–420. https://doi.org/10.1016/j.jenvman.2007.10.010.

[87] Y. Yang, H. Zhang, Y. Yan, Preparation of novel iron-loaded microfibers entrapped carbon-nanotube composites for catalytic wet peroxide oxidation of m-cresol in a fixed bed reactor, Sep. Purif. Technol. 212 (2019) 405–415. https://doi.org/10.1016/j.seppur.2018.11.050.

[88] J. Qian, K. Wang, Q. Guan, H. Li, H. Xu, Q. Liu, W. Liu, B. Qiu, Enhanced wet hydrogen peroxide catalytic oxidation performances based on CuS nanocrystals / reduced graphene oxide composites, Appl. Surf. Sci. 288 (2014) 633–640. https://doi.org/10.1016/j.apsusc.2013.10.086.

[89] Y. Yang, H. Zhang, Y. Yan, Catalytic wet peroxide oxidation of m-cresol over novel Fe_2O_3 loaded microfibrous entrapped CNT composite catalyst in a fixed-bed reactor, J.

Chem. Technol. Biotechnol. 93 (2018) 2552–2563. https://doi.org/10.1002/jctb.5609.

[90] E. Lorençon, D.C. Ferreira, R.R. Resende, K. Krambrock, Amphiphilic gold nanoparticles supported on carbon nanotubes: Catalysts for the oxidation of lipophilic compounds by wet peroxide in biphasic systems, Appl. Catal. A Gen. 505 (2015) 566–574. https://doi.org/10.1016/j.apcata.2015.05.016.

[91] W. Liu, J. Qian, K. Wang, H. Xu, D. Jiang, Q. Liu, X. Yang, H. Li, Magnetically Separable Fe_3O_4 Nanoparticles-Decorated Reduced Graphene Oxide Nanocomposite for Catalytic Wet Hydrogen Peroxide Oxidation, J. Inorg. Organomet. Polym. Mater. 23 (2013) 907–916. https://doi.org/10.1007/s10904-013-9863-4.

[92] Y. Huaccallo, S. Álvarez-Torrellas, M.P. Marín, M.V. Gil, M. Larriba, V.I. Águeda, G. Ovejero, J. García, Magnetic Fe_3O_4/multi-walled carbon nanotubes materials for a highly efficient depletion of diclofenac by catalytic wet peroxideoxidation, Environ. Sci. Pollut. Res. 26 (2019) 22372–22388. https://doi.org/10.1007/s11356-019-05597-x.

[93] H.Y. Xu, Y. Wang, T.N. Shi, H. Zhao, Q. Tan, B.C. Zhao, X.L. He, S.Y. Qi, Heterogeneous Fenton-like discoloration of methyl orange using Fe_3O_4/MWCNTs as catalyst: combination mechanism and affecting parameters, Front. Mater. Sci. 12 (2018) 21–33. https://doi.org/10.1007/s11706-018-0408-1.

[94] A. Rodríguez, G. Ovejero, J.L. Sotelo, M. Mestanza, J. García, Heterogeneous fenton catalyst supports screening for mono azo dye degradation in contaminated wastewaters, Ind. Eng. Chem. Res. 49 (2010) 498–505. https://doi.org/10.1021/ie901212m.

[95] F. Liu, H. Zhang, Y. Yan, H. Huang, Graphene as efficient and robust catalysts for catalytic wet peroxide oxidation of phenol in a continuous fixed-bed reactor, Sci. Total Environ. 701 (2020) 134772. https://doi.org/10.1016/j.scitotenv.2019.134772.

[96] R.S. Ribeiro, A.M.T. Silva, J.L. Figueiredo, J.L. Faria, H.T. Gomes, Removal of 2-nitrophenol by catalytic wet peroxide oxidation using carbon materials with different morphological and chemical properties, Appl. Catal. B Environ. 140–141 (2013) 356–362. https://doi.org/10.1016/j.apcatb.2013.04.031.

[97] R.S. Ribeiro, A.M.T. Silva, L.M. Pastrana-Martínez, J.L. Figueiredo, J.L. Faria, H.T. Gomes, Graphene-based materials for the catalytic wet peroxide oxidation of highly concentrated 4-nitrophenol solutions, Catal. Today. 249 (2015) 204–212. https://doi.org/10.1016/j.cattod.2014.10.004.

[98] M. Soria-Sánchez, E. Castillejos-López, A. Maroto-Valiente, M.F.R. Pereira, J.J.M. Órfão, A. Guerrero-Ruiz, High efficiency of the cylindrical mesopores of MWCNTs

for the catalytic wet peroxide oxidation of C.I. Reactive Red 241 dissolved in water, Appl. Catal. B Environ. 121–122 (2012) 182–189. https://doi.org/10.1016/j.apcatb.2012.04.004.

[99] K. Huang, Y. Xu, Enhancing the catalytic behaviour of HKUST-1 by graphene oxide for phenol oxidation, Environ. Technol. 0 (2019) 1–11. https://doi.org/10.1080/09593330.2019.1643410.

[100] Y. Huaccallo-Aguilar, S. Álvarez-Torrellas, M. Larriba, V.I. Águeda, J.A. Delgado, G. Ovejero, J. García, Optimization parameters, kinetics and mechanism of naproxen removal by catalytic wet peroxide oxidation with a hybrid iron-based magnetic catalyst, Catalysts. 9 (2019) 1–23. https://doi.org/10.3390/catal9030287.

[101] N.A. Fathy, S.E. El-Shafey, O.I. El-Shafey, Synthesis of a novel MnO_2@carbon nanotubes-graphene hybrid catalyst (MnO_2@CNT-G) for catalytic oxidation of basic red 18 dye (BR18), J. Water Process Eng. 17 (2017) 95–101. https://doi.org/10.1016/j.jwpe.2017.03.010.

[102] Z. Ye, Y. Jiang, J. Qian, W. Li, T. Feng, L. Li, F. Wu, R. Chen, Exceptional adsorption and catalysis effects of hollow polyhedra/carbon nanotube confined CoP nanoparticles superstructures for enhanced lithium–sulfur batteries, Nano Energy. 64 (2019) 1–10. https://doi.org/10.1016/j.nanoen.2019.103965.

[103] C. Li, X. Zhang, K. Wang, F. Su, C.-M. Chen, F. Liu, Z.-S. Wu, Y. Ma, Recent advances in carbon nanostructures prepared from carbon dioxide for high-performance supercapacitors, J. Energy Chem. 54 (2020) 352–367. https://doi.org/10.1016/j.jechem.2020.05.058.

[104] W. Zhu, D. Lei, Y. Li, F. Zhang, J. Guo, Hierarchical, nitrogenous hollow carbon spheres filled with porous carbon nanosheets for use as efficient sulfur hosts for lithium-sulfur batteries, J. Alloys Compd. 836 (2020) 155295. https://doi.org/10.1016/j.jallcom.2020.155295.

[105] C. Huang, C. Li, G. Shi, Graphene based catalysts, Energy Environ. Sci. 5 (2012) 8848–8868. https://doi.org/10.1039/c2ee22238h.

[106] K.S. Novoselov, A.K. Geim, S. V. Morozov, D. Jiang, Y. Zhang, S. V. Dubonos, I. V. Grigorieva, A.A. Firsov, Electric Field Effect in Atomically Thin Carbon Films, Science (80-.). 306 (2004) 666–669. https://doi.org/10.1126/science.1102896.

[107] W.W. Liu, S.P. Chai, A.R. Mohamed, U. Hashim, Synthesis and characterization of graphene and carbon nanotubes: A review on the past and recent developments, J. Ind. Eng. Chem. 20 (2014) 1171–1185. https://doi.org/10.1016/j.jiec.2013.08.028.

[108] T.C. Dinadayalane, J. Leszczynski, Remarkable diversity of carbon – carbon bonds : structures and properties of fullerenes, carbon nanotubes, and graphene, Struct Chem. (2010) 1155–1169. https://doi.org/10.1007/s11224-010-9670-2.

[109] B. Yan, Z. Hiew, L. Yee, X. Jiat, S. Gan, S. Thangalazhy-gopakumar, S. Shee, G. Pan, T.C. Yang, Adsorptive removal of diclofenac by graphene oxide: Optimization, equilibrium, kinetic and thermodynamic studies, J. Taiwan Inst. Chem. Eng. 98 (2019) 150–162. https://doi.org/10.1016/j.jtice.2018.07.034.

[110] S. Iijima, Helical microtubules of graphitic carbon, Nature. 354 (1991) 56–58. https://doi.org/10.1038/354056a0.

[111] N. Hiremath, G. Bhat, High-performance carbon nanofibers and nanotubes, in: G. Bhat (Ed.), Struct. Prop. High-Performance Fibers, Woodhead Publishing, 2017: pp. 79–109. https://doi.org/10.1016/B978-0-08-100550-7.00004-8.

[112] J. Leszczynski, T.C. Dinadayalane, Fundamental Structural, Electronic, and Chemical Properties of Carbon Nanostructures: Graphene, Fullerenes, Carbon Nanotubes, and TheirDerivatives, 2017. https://doi.org/10.1007/978-3-319-27282-5.

[113] D.S. Bethune, C.H. Klang, M.S. De Vries, G. Gorman, R. Savoy, J. Vazquez, R. Beyers, Cobalt-catalysed growth of carbon nanotubes with single-atomic-layer walls, Nature. 363 (1993) 605–607. https://doi.org/10.1038/363605a0.

[114] P. Serp, J.L. Figueiredo, Carbon Materials for Catalysis, 1st ed., Wiley, New Jersey, 2009.

[115] P. J.F.Harris, Carbon Nanotubes and Related Structures: New Materials for the Twenty-first Century, Cambridge University Press, 1999. https://doi.org/10.1017/CBO9780511605819.

[116] M.L. Wang, W.F. Bian, The relationship between the mechanical properties and microstructures of carbon fibers, New Carbon Mater. 35 (2020) 42–49. https://doi.org/10.1016/S1872-5805(20)60474-7.

[117] I.U. Din, M.S. Shaharun, A. Naeem, M.A. Alotaibi, A.I. Alharthi, M.A. Bakht, Q. Nasir, Carbon nanofibers as potential materials for catalysts support, a mini-review on recent advances and future perspective, Ceram. Int. 46 (2020) 18446–18452. https://doi.org/10.1016/j.ceramint.2020.04.275.

[118] M. Martin-Martinez, B.F. Machado, P. Serp, S. Morales-Torres, A.M.T. Silva, J.L. Figueiredo, J.L. Faria, H.T. Gomes, Carbon nanotubes as catalysts for wet peroxide oxidation: The effect of surface chemistry, Catal. Today. (2019) 1–9. https://doi.org/10.1016/j.cattod.2019.03.014.

[119] A. Thess, R. Lee, P. Nikolaev, H. Dai, P. Petit, J. Robert, C. Xu, Y.H. Lee, S.G. Kim, A.G. Rinzler, D.T. Colbert, G.E. Scuseria, D. Tomanek, J.E. Fischer, R.E. Smalley, Crystalline Ropes of Metallic Carbon Nanotubes, Cryst. Ropes Met. Carbon Nanotub. 273 (1996) 483–487. https://doi.org/10.1126/science.273.5274.483.

[120] L.M. Liz-Marzán, P. V. Kamat, Nanoscale Materials, Kluwer, Boston, 2004.

[121] K. Koziol, B.O. Boskovic, N. Yahya, Synthesis of Carbon Nanostructures by CVD Method, in: Carbon and Oxide Nanostructures, Springer, Berlin, Heidelberg, 2010: pp. 23–49. https://doi.org/10.1007/8611_2010_12.

[122] K.A. Shah, B.A. Tali, Synthesis of carbon nanotubes by catalytic chemical vapour deposition: A review on carbon sources, catalysts and substrates, Mater. Sci. Semicond. Process. 41 (2016) 67–82. https://doi.org/10.1016/j.mssp.2015.08.013.

[123] Ç. Öncel, Y. Yürüm, Carbon nanotube synthesis via the catalytic CVD method: A review on the effect of reaction parameters, Fullerenes Nanotub. Carbon Nanostructures. 14 (2006) 17–37. https://doi.org/10.1080/15363830500538441.

[124] G.S. Bajad, R.P. Vijayakumar, A.G. Gupta, V. Jagtap, Y. pal Singh, Production of liquid hydrocarbons, carbon nanotubes and hydrogen rich gases from waste plastic in a multi-core reactor, J. Anal. Appl. Pyrolysis. 125 (2017) 83–90. https://doi.org/10.1016/j.jaap.2017.04.016.

[125] M. Kumar, Y. Ando, Chemical vapor deposition of carbon nanotubes: A review on growth mechanism and mass production, J. Nanosci. Nanotechnol. 10 (2010) 3739–3758. https://doi.org/10.1166/jnn.2010.2939.

[126] G. Ortega-Cervantez, G. Rueda-Morales, J. Ortiz-López, Catalytic CVD production of carbon nanotubes using ethanol, Microelectronics J. 36 (2005) 495–498. https://doi.org/10.1016/j.mejo.2005.02.062.

[127] N. Tripathi, P. Mishra, H. Harsh, S.S. Islam, Fine-tuning control on CNT diameter distribution, length and density using thermal CVD growth at atmospheric pressure: an in-depth analysis on the role of flow rate and flow duration of acetylene (C_2H_2) gas, Appl. Nanosci. 5 (2015) 19–28. https://doi.org/10.1007/s13204-013-0288-8.

[128] The World Bank, Trends in Solid Waste Management, WHAT A WASTE 2.0. (n.d.). https://datatopics.worldbank.org/what-a-waste/trends_in_solid_waste_management.html (accessed July 23, 2020).

[129] Statista, Projected generation of municipal solid waste worldwide from 2016 to 2050, (2018). https://www.statista.com/statistics/916625/global-generation-of-municipal-solid-waste-forecast/ (accessed July 23, 2020).

[130] The World Bank, Five ways cities can curb plastic waste, (2018). https://blogs.worldbank.org/sustainablecities/five-ways-cities-can-curb-plastic-waste (accessed July 23, 2020).

[131] The World Bank, Solid Waste Management, (2019). https://www.worldbank.org/en/topic/urbandevelopment/brief/solid-waste-management (accessed August 19, 2020).

[132] P.R. Yaashikaa, P.S. Kumar, A. Saravanan, S. Varjani, R. Ramamurthy, Bioconversion of municipal solid waste into bio-based products: A review on valorisation and sustainable approach for circular bioeconomy, Sci. Total Environ. 748 (2020) 141312. https://doi.org/10.1016/j.scitotenv.2020.141312.

[133] S. Wang, W. Yan, F. Zhao, Recovery of solid waste as functional heterogeneous catalysts for organic pollutant removal and biodiesel production, Chem. Eng. J. 401 (2020) 126104. https://doi.org/10.1016/j.cej.2020.126104.

[134] A.A. Koutinas, A. Vlysidis, D. Pleissner, N. Kopsahelis, I. Lopez Garcia, I.K. Kookos, S. Papanikolaou, T.H. Kwan, C.S.K. Lin, Valorization of industrial waste and by-product streams via fermentation for the production of chemicals and biopolymers, Chem. Soc. Rev. 43 (2014) 2587–2627. https://doi.org/10.1039/c3cs60293a.

[135] S.S. Sharma, V.S. Batra, Production of hydrogen and carbon nanotubes via catalytic thermo-chemical conversion of plastic waste: review, J. Chem. Technol. Biotechnol. 95 (2020) 11–19. https://doi.org/10.1002/jctb.6193.

[136] A. Bazargan, G. McKay, A review - Synthesis of carbon nanotubes from plastic wastes, Chem. Eng. J. 195–196 (2012) 377–391. https://doi.org/10.1016/j.cej.2012.03.077.

[137] H. Ago, S. Ohshima, K. Uchida, M. Yumura, Gas-phase synthesis of single-wall carbon nanotubes from colloidal solution of metal nanoparticles, J. Phys. Chem. B. 105 (2001) 10453–10456. https://doi.org/10.1021/jp012084j.

[138] C. Singh, M.S.P. Shaffer, A.H. Windle, Production of controlled architectures of aligned carbon nanotubes by an injection chemical vapour deposition method, Carbon N. Y. 41 (2003) 359–368. https://doi.org/10.1016/S0008-6223(02)00314-7.

[139] M. Karimi, J.L. Diaz de Tuesta, C.N. Carmem, H.T. Gomes, A.E. Rodrigues, J.A.C. Silva, Compost from Municipal Solid Wastes as a Source of Biochar for CO_2 Capture, Chem. Eng. Technol. 43 (2020) 1336–1349. https://doi.org/10.1002/ceat.201900108.

[140] M. Thommes, K. Kaneko, A. V. Neimark, J.P. Olivier, F. Rodriguez-Reinoso, J. Rouquerol, K.S.W. Sing, Physisorption of gases, with special reference to the

evaluation of surface area and pore size distribution (IUPAC Technical Report), Pure Appl. Chem. 87 (2015) 1051–1069. https://doi.org/10.1515/pac-2014-1117.

[141] J. Cardoso, H.T. Gomes, P. Brito, Viability of the use of leachates from a mechanical biological municipal solid waste treatment plant as fertilizers, Recycling. 4 (2019). https://doi.org/10.3390/recycling4010008.

[142] C.M. Masso, H.T. Gomes, J.M.T. Pietrobelli, J.L.D. De Tuesta, Valorization of compost in the production of carbon-based materials for the treatment of contaminated wastewater Valorization of compost in the production of carbon-based materials for the treatment of contaminated wastewater, 2018.

[143] G.M. Eisenberg, Colorimetric Determination of Hydrogen Peroxide, Ind. Eng. Chem. - Anal. Ed. 15 (1943) 327–328. https://doi.org/10.1021/i560117a011.

[144] J.B. de H. Alonso, J.T. Antón, T.G. Montero, J.R.D. Vargas, Análisis químico de aguas residuales, @becedario, 2004.

[145] J.D. Box, Investigation of the Folin-Ciocalteau phenol reagent for the determination of polyphenolic substances in natural waters, Water Res. 17 (1983) 511–525. https://doi.org/10.1016/0043-1354(83)90111-2.

[146] J. Xu, H. Yang, W. Fu, K. Du, Y. Sui, J. Chen, Y. Zeng, M. Li, G. Zou, Preparation and magnetic properties of magnetite nanoparticles by sol-gel method, J. Magn. Magn. Mater. 309 (2007) 307–311. https://doi.org/10.1016/j.jmmm.2006.07.037.

[147] P. Daniel, S.I. Shylin, H. Lu, M.N. Tahir, M. Panthöfer, T. Weidner, A. Möller, V. Ksenofontov, W. Tremel, The surface chemistry of iron oxide nanocrystals: Surface reduction of γ-Fe_2O_3 to Fe_3O_4 by redox-active catechol surface ligands, J. Mater. Chem. C. 6 (2018) 326–333. https://doi.org/10.1039/c7tc04795a.

[148] A. Aharoni, E.H. Frei, M. Schieber, Some properties of γ-Fe_2O_3 obtained by hydrogen reduction of α-Fe_2O_3, J. Phys. Chem. Solids. 23 (1962) 545–554. https://doi.org/10.1016/0022-3697(62)90512-7.

[149] A. Veksha, A. Giannis, V.W.C. Chang, Conversion of non-condensable pyrolysis gases from plastics into carbon nanomaterials: Effects of feedstock and temperature, J. Anal. Appl. Pyrolysis. 124 (2017) 16–24. https://doi.org/10.1016/j.jaap.2017.03.005.

[150] J.C. Acomb, C. Wu, P.T. Williams, Control of steam input to the pyrolysis-gasification of waste plastics for improved production of hydrogen or carbon nanotubes, Appl. Catal. B Environ. 147 (2014) 571–584. https://doi.org/10.1016/j.apcatb.2013.09.018.

[151] C. Zhuo, B. Hall, H. Richter, Y. Levendis, Synthesis of carbon nanotubes by sequential pyrolysis and combustion of polyethylene, Carbon N. Y. 48 (2010) 4024–

4034. https://doi.org/10.1016/j.carbon.2010.07.007.

[152] X. Wang, Z. Zhao, J. Qu, Z. Wang, J. Qiu, Fabrication and characterization of magnetic Fe_3O_4-CNT composites, J. Phys. Chem. Solids. 71 (2010) 673–676. https://doi.org/10.1016/j.jpcs.2009.12.063.

[153] S. Kazemifard, H. Nayebzadeh, N. Saghatoleslami, E. Safakish, Assessment the activity of magnetic KOH/Fe_3O_4@Al_2O_3 core–shell nanocatalyst in transesterification reaction: effect of Fe/Al ratio on structural and performance, Environ. Sci. Pollut. Res. 25 (2018) 32811–32821. https://doi.org/10.1007/s11356-018-3249-7.

[154] S. Shi, C. Xu, X. Wang, Y. Xie, Y. Wang, Q. Dong, L. Zhu, G. Zhang, D. Xu, Electrospinning fabrication of flexible Fe_3O_4 fibers by sol-gel method with high saturation magnetization for heavy metal adsorption, Mater. Des. 186 (2020) 108298. https://doi.org/10.1016/j.matdes.2019.108298.

[155] V. Ţucureanu, A. Matei, A.M. Avram, FTIR Spectroscopy for Carbon Family Study, Crit. Rev. Anal. Chem. 46 (2016) 502–520. https://doi.org/10.1080/10408347.2016.1157013.

[156] F. Tsegaye, A.M. Taddesse, E. Teju, M. Aschalew, Preparation and sorption property stufy of Fe_3O_4/Al_2O_3/ZrO_2 composite for the removal of cadmium, lead and chromium ions from aqueous solutions, Bull. Chem. Soc. Ethiop. 34 (2020) 105–121. https://doi.org/10.4314/bcse.v34i1.10.

[157] A. Hadi, J. Zahirifar, J. Karimi-Sabet, A. Dastbaz, Graphene nanosheets preparation using magnetic nanoparticle assisted liquid phase exfoliation of graphite: The coupled effect of ultrasound and wedging nanoparticles, Ultrason. Sonochem. 44 (2018) 204–214. https://doi.org/10.1016/j.ultsonch.2018.02.028.

[158] S. Bandi, S. Ravuri, D.R. Peshwe, A.K. Srivastav, Graphene from discharged dry cell battery electrodes, J. Hazard. Mater. 366 (2019) 358–369. https://doi.org/10.1016/j.jhazmat.2018.12.005.

[159] K.S.W. Sing, R.T. Williams, Physisorption hysteresis loops and the characterization of nanoporous materials, Adsorpt. Sci. Technol. 22 (2004) 773–782. https://doi.org/10.1260/0263617053499032.

[160] K.A. Cychosz, R. Guillet-Nicolas, J. García-Martínez, M. Thommes, Recent advances in the textural characterization of hierarchically structured nanoporous materials, Chem. Soc. Rev. 46 (2017) 389–414. https://doi.org/10.1039/c6cs00391e.

[161] N. Dolfini, Avaliação da remoção de amoxicilina por adsorção em carvão ativado de origem mineral, Universidade Estadual de Maringá, 2018.

[162] B. Strzemiecka, A. Voelkel, J. Donate-Robles, J.M. Martín-Martínez, Assessment of the surface chemistry of carbon blacks by TGA-MS, XPS and inverse gas chromatography using statistical chemometric analysis, Appl. Surf. Sci. 316 (2014) 315–323. https://doi.org/10.1016/j.apsusc.2014.07.174.

[163] J.T. Yeh, T.W. Wu, Y.C. Lai, H.P. Zhou, Q. Zhou, Q.C. Li, S. Wen, F.C. Tsai, C.Y. Huang, K.S. Huang, K.N. Chen, Ultradrawing properties of ultra-high molecular weight polyethylene/ functionalized carbon nanotube fibers, Polym. Eng. Sci. 51 (2011) 687–696. https://doi.org/10.1002/pen.21871.

[164] J. Zhang, J. Du, Y. Qian, S. Xiong, Synthesis, characterization and properties of carbon nanotubes microspheres from pyrolysis of polypropylene and maleated polypropylene, Mater. Res. Bull. 45 (2010) 15–20. https://doi.org/10.1016/j.materresbull.2009.09.007.

[165] A.S. Silva, M.S. Kalmakhanova, B.K. Massalimova, J.L.D. de Tuesta, H.T. Gomes, Wet peroxide oxidation of paracetamol using acid activated and Fe/Co-pillared clay catalysts prepared from natural clays, Catalysts. 9 (2019). https://doi.org/10.3390/catal9090705.

[166] N. Barrios-Bermúdez, M. González-Avendaño, I. Lado-Touriño, A. Cerpa-Naranjo, M.L. Rojas-Cervantes, Fe-Cu doped multiwalled carbon nanotubes for fenton-like degradation of paracetamol under mild conditions, Nanomaterials. 10 (2020) 11–13. https://doi.org/10.3390/nano10040749.

[167] E. Moctezuma, E. Leyva, C.A. Aguilar, R.A. Luna, C. Montalvo, Photocatalytic degradation of paracetamol: Intermediates and total reaction mechanism, J. Hazard. Mater. 243 (2012) 130–138. https://doi.org/10.1016/j.jhazmat.2012.10.010.

[168] N. Villota, J.M. Lomas, L.M. Camarero, Study of the paracetamol degradation pathway that generates color and turbidity in oxidized wastewaters by photo-Fenton technology, J. Photochem. Photobiol. A Chem. 329 (2016) 113–119. https://doi.org/10.1016/j.jphotochem.2016.06.024.